Nonlinear H ∞ -control under unilateral constraints

Oscar Montano, Y Orlov, Y Aoustin

Nonlinear $\mathcal{H}_\infty$-control under unilateral constraints

O.E. Montano[a], Y. Orlov[a*] and Y. Aoustin[b]

[a]*Department of Electronics and Telecommunications, Center for Scientific Research and Higher Education at Ensenada, Baja California, Carretera Ensenada-Tijuana No. 3918, Zona Playitas, C.P. 22860, Ensenada, B.C., Mexico. Email: omontano@cicese.edu.mx, yorlov@cicese.mx;* [b]*L'UNAM, Institut de Recherche en Communications et Cybernétique de Nantes UMR CNRS 6597, CNRS, Université de Nantes, Ecole Centrale de Nantes, 1 rue de la Noë, 44321 Nantes Cedex 3, France. Email: yannick.aoustin@irccyn.ec-nantes.fr*

(*August 2015*)

The primary concern of the work is robust control of hybrid mechanical systems under unilateral constraints of co-dimension one. Nonlinear $\mathcal{H}_\infty$ output feedback synthesis is developed in the hybrid setting, covering collision phenomena. Robustness issues of the proposed synthesis are numerically illustrated in two benchmark applications. First, the regulation and orbital stabilization of a simple mass-spring-damper system, impacting a barrier, illustrate the capability of the proposed approach via state feedback and position feedback designs, respectively. In order to add a practical value to the present investigation the tracking synthesis of a walking gait is then addressed for a complex bipedal robot with feet. In both applications, good performances are achieved despite imperfect measurements and the presence of both external disturbances, affecting the collision-free motion phase, and uncertainties that occur in the collision phase.

Keywords: robust control, unilateral constraints, mechanical systems, orbital stabilization, disturbance attenuation.

Funding

*Corresponding author. Email: yorlov@cicese.mx

1.   Introduction

Significant research interest has been devoted to the stability analysis and control synthesis of switched systems subject to input, state and output constraints. The progress made in the area relied on different tools such as multiple Lyapunov functions (**?**) and predictive control (**?**) among others. More recently, barrier Lyapunov functions (functions which grow to infinity when their arguments approach the domain boundaries) have been involved into the tracking control synthesis of nonlinear switched systems with output constraints (**????**). Sliding mode control of switched single-input, output-constrained systems have also been brought into play (**?**). In addition, robustness of linear switched systems subject to actuator constraints has been studied in (**?**) in terms of the $\mathcal{L}_2$-gain, using the LMI-optimization approach. A piece-wise linear $\mathcal{H}_\infty$ control synthesis was developed for switched systems with output constraints in (**?**), relying again on the LMI-optimization.

Switched dynamic systems, which are governed by continuous differential equations and difference equations provided that the switch between such equations is defined according to output and/or time constraints, are typically referred to as hybrid systems. Such systems have also attracted a lot of attention due to the wide variety of their applications and due to the need of special analysis tools for this type of systems. The interested reader may refer to the relevant works by **????**, to name a few. Particularly, the disturbance attenuation problem for hybrid dynamic systems has been addressed by **???** where impulsive control inputs were admitted to counteract/compensate disturbances/uncertainties at time instants of instantaneous changes of the underlying state. It should be noted, however, that even in the state feedback design, a pair of independent Riccati equations, separately coming from continuous and discrete dynamics, was required to possess a solution that satisfies both equations. A restrictive condition was thus involved on the feasibility of the proposed synthesis. Moreover, the physical implementation of impulsive control inputs was impossible in many practical situations, e.g., while controlling walking biped robots.

Thus motivated, the present investigation intends to introduce a new control strategy, which is feasible under certain conditions and which avoids using impulsive control inputs. The control objective in the question is to asymptotically stabilize the undisturbed hybrid system, while also attenuating external disturbances. The work focuses on impact hybrid systems, which are recognized as dynamic systems under unilateral constraints (**?**). Since the dynamic systems with unilateral constraints possess nonsmooth solutions, which arise due to hitting the constraints, a challenging problem is to extend the popular nonlinear $\mathcal{H}_\infty$ approach (**???**) to this kind of dynamic systems. It is worth noticing that the Lyapunov characterization of integral Input-to-State Stability (iISS), recently developed by **?** for impulsive systems with state-independent impacts, could form a basis for such an extension. However, choosing this route would call for further generalization of iISS concept to hybrid systems (possibly under unilateral constraints) with state-dependent impacts.

The $\mathcal{H}_\infty$ approach, that has recently been developed by **?** towards nonsmooth mechanical applications with hard-to-model friction forces and backlash effects, is now extended in the presence of unilateral constraints. Such an extension, recently reported by **?** for tracking control of a simple 1-DOF (degree-of-freedom) mechanical system, constitutes a part of this work and it is further generalized to multi-link mechanical systems with unilateral constraints of co-dimension 1. The general case of unilateral constraints of higher co-dimensions, possibly, resulting in ill-posed dynamics (**??**), remains beyond the scope of the present investigation.

Both the full information case with perfect state measurements and the incomplete information case with output disturbance-corrupted measurements are addressed and specified for n-DOF fully actuated mechanical manipulators. An essential feature, adding the value to the present investigation, is that not only standard external disturbances, but also their discrete-time counterparts are attenuated with the proposed synthesis. This feature has successfully been justified *ad hoc* while testing the robust tracking synthesis of a stable biped periodic gait (**??**). It is worth noticing that this is in contrast to the control algorithms, developed so far (cf. that of **?**) where the perfect

knowledge of the restitution rule is assumed at the collision time instants.

To facilitate the exposition capabilities of the developed synthesis and its robustness features are first illustrated with a simple linear 1-DOF mass-spring-damper system, impacting against a barrier. In addition to the numerical study, made for the state feedback regulation of this Mass-Spring-Damper-Barrier (MSDB) testbed, two different scenarios are invented and tested side by side for the MSDB position feedback tracking of an impact reference model, generating a stable limit cycle. In the first scenario, an impact reference output to follow is constructed off-line based on the impact Van der Pol oscillator (?). In the second scenario, the same reference output is updated on-line to synchronize its impacts to the time instants when the plant hits the unilateral constraint. As theoretically predicted, the disturbance attenuation is actually enforced and good performance of the closed-loop system is concluded from the numerical study being conducted for the former scenario. However, the disturbance-free closed-loop system proves to be asymptotically unstable because of the potential impact desynchronization (?). In the latter scenario, the reference trajectory tracking is tested under on-line synchronization of the reference velocity jumps to the collision time instants of the plant. Simulation runs are additionally conducted for this scenario to support the theory in that the closed-loop system is capable of retaining attractive robustness features while also presenting the asymptotic stability in the disturbance-free environment.

In order to add the practical value to the present development it is additionally applied to the orbital stabilization of a seven-link bipedal robot with feet required to track a walking gait which is composed of single support phases separated by impacts. The numerical study, made on the biped emulator from (?), supports good robustness features of the proposed orbital synthesis against both external disturbances, affecting the collision-free motion phase, and against uncertainties that occur in the collision phase.

Being numerically justified in the above benchmark testbeds, the robustness features of the proposed synthesis form the novelty of the paper along with the theoretical development of the nonsmooth $\mathcal{H}_\infty$ framework under unilateral constraints. The contribution of the paper into the existing literature is thus twofold. First, the nonlinear $\mathcal{H}_\infty$ approach is constructively generalized under unilateral constraints by means of incorporating an additional condition on the plant reset in the closed-loop. The resulting robust synthesis is then effectively applied to the afore-given benchmark impact testbeds, operating under both external disturbances and restitution uncertainties, for the purpose of generating periodic motions. Application to the robust tracking synthesis of a stable biped periodic gate, validated on a real-life biped emulator, is of its own value.

The paper is outlined as follows. Section 2 presents a hybrid model of interest which is subject to a unilateral constraint. The $\mathcal{H}_\infty$-control problem is then stated for such a system. Section 3 derives sufficient conditions for a local solution of the underlying problem to exist, and an output feedback controller is additionally synthesized. In Section 4, the resulting synthesis is applied to n-DOF mechanical manipulators subject to unilateral constraints and its capabilities are illustrated in Section ?? in numerical experiments made for the regulation and orbital stabilization of the impact MSDB testbed. Section ?? presents the numerical results of the application of the developed synthesis to the orbital stabilization of a seven-link bipedal robot with feet. Finally, conclusions are collected in Section ??.

1.1 *Notation*

The notation used throughout is rather standard. The argument t^+ is used to denote the right-hand side value $\mathbf{x}(t^+)$ of a trajectory $\mathbf{x}(t)$ at an impact time instant t whereas $\mathbf{x}(t^-)$ stands for the left-hand side value of the same; by default, $\mathbf{x}(t)$ is reserved for $\mathbf{x}(t^-)$, thus implying an underlying trajectory to be continuous on the left.

2.   Problem Statement

Given a scalar time-varying unilateral constraint $F(\mathbf{x_1}, t) \geq 0$, consider a non-autonomous nonlinear system, evolving within the above constraint, which is governed by continuous dynamics of the form

$$
\begin{aligned}
\dot{\mathbf{x}}_1 &= \mathbf{x}_2 \\
\dot{\mathbf{x}}_2 &= \mathbf{\Phi}(\mathbf{x}_1, \mathbf{x}_2, t) + \mathbf{\Psi_1}(\mathbf{x}_1, \mathbf{x}_2, t)\mathbf{w} + \mathbf{\Psi_2}(\mathbf{x}_1, \mathbf{x}_2, t)\mathbf{u}
\end{aligned}
\tag{1}
$$

$$
\mathbf{z} = \mathbf{h_1}(\mathbf{x}_1, \mathbf{x}_2, t) + \mathbf{k_{12}}(\mathbf{x}_1, \mathbf{x}_2, t)\mathbf{u}
\tag{2}
$$

$$
\mathbf{y} = \mathbf{h_2}(\mathbf{x}_1, \mathbf{x}_2, t) + \mathbf{k_{21}}(\mathbf{x}_1, \mathbf{x}_2, t)\mathbf{w}
\tag{3}
$$

beyond the surface $F(\mathbf{x_1}, t) = 0$ when the constraint is inactive, and by the algebraic relations

$$
\begin{aligned}
\mathbf{x}_1(t_i^+) &= \mathbf{x}_1(t_i^-) \\
\mathbf{x}_2(t_i^+) &= \boldsymbol{\mu}_0(\mathbf{x}_1(t_i), \mathbf{x}_2(t_i^-), t_i) + \boldsymbol{\omega}(\mathbf{x}_1(t_i), \mathbf{x}_2(t_i^-), t_i)\mathbf{w_i^d}
\end{aligned}
\tag{4}
$$

$$
\mathbf{z_i^d} = \mathbf{x}_2(t_i^+)
\tag{5}
$$

at *a priori* unknown collision time instants $t = t_i$, $i = 1, 2, \ldots$, when the system trajectory hits the surface $F(\mathbf{x_1}, t) = 0$.

In the above relations, $\mathbf{x}^\top = [\mathbf{x}_1^\top, \mathbf{x}_2^\top] \in \mathbb{R}^{2n}$ represents the state vector with components $\mathbf{x}_1 \in \mathbb{R}^n$ and $\mathbf{x}_2 \in \mathbb{R}^n$; $\mathbf{u} \in \mathbb{R}^n$ is the control input of dimension n; $\mathbf{w} \in \mathbb{R}^l$ and $\mathbf{w_i^d} \in \mathbb{R}^q$ collect exogenous signals affecting the motion of the system (external forces, including impulsive ones, as well as model and measurement imperfections). The variable $\mathbf{y} \in \mathbb{R}^p$ is the only available measurement of the state of the system whereas the variables $\mathbf{z} \in \mathbb{R}^m$ and $\mathbf{z_i^d} \in \mathbb{R}^n$ represent the outputs of the system to be controlled. Since impulsive control actions were ruled out, the post-impact value $\mathbf{x}_2(t)$ of the state component subject to the instantaneous change was chosen as a discrete output function $\mathbf{z_i^d}$.

Throughout, the matrix functions $\mathbf{\Phi}$, $\mathbf{\Psi_1}$, $\mathbf{\Psi_2}$, $\mathbf{h_1}$, $\mathbf{k_{12}}$, $\mathbf{k_{21}}$, F, $\boldsymbol{\mu}_0$, and $\boldsymbol{\omega}$ are of appropriate dimensions, which are continuously differentiable in their arguments and uniformly bounded in t. Admitting these functions to be time-varying is particularly invoked to deal with tracking problems where the plant description is given in terms of the state deviation from the reference trajectory to track (?). In addition, the origin is assumed to be an equilibrium of the unforced system (1)-(5), i.e., for all t, one has $\mathbf{\Phi}(\mathbf{0}, \mathbf{0}, t) = \mathbf{0}$, $\mathbf{h_1}(\mathbf{0}, \mathbf{0}, t) = \mathbf{0}$, $\mathbf{h_2}(\mathbf{0}, \mathbf{0}, t) = \mathbf{0}$, and $\boldsymbol{\mu}_0(\mathbf{0}, \mathbf{0}, t) = \mathbf{0}$.

Clearly, the above system (1)-(5) is an affine control system of the vector relative degree $[2, \ldots, 2]^\top$ and it governs a wide class of mechanical systems with impacts. Since the control input $\mathbf{u}$ has the same dimension as that of the generalized position $\mathbf{x}$ the present investigation is confined to the fully actuated case, though it could readily be extended to the over-actuated case with a correct choice of the control inputs. The treatment in the underactuated case is also possible using the virtual constraint approach (??) whenever it is applicable (e.g., for the undegraduation degree one similar to that of ?).

If interpreted in terms of mechanical systems, equation (1) describes the continuous dynamics before the underlying system hits the reset surface $F(\mathbf{x_1}, t) = 0$, which depends on the position and time variables only. In turn, the restitution law, given by equation (4), is a physical law for the instantaneous change of the velocity when the resetting surface is hit. Thus, the position is not instantaneously changed at the collision time instants whereas the post-impact velocity $\mathbf{x}_2(t^+)$ is

a function of both the pre-impact state $(\mathbf{x_1}(t), \mathbf{x_2}(t^-))$ and a discrete perturbation $\mathbf{w_d}$ accounting for inadequacies of the restitution law.

For later use, the notion of an admissible controller is specified for the underlying system. Consider a causal dynamic feedback controller of the same structure

$$\dot{\boldsymbol{\xi}}_1 = \boldsymbol{\xi}_2, \quad \dot{\boldsymbol{\xi}}_2 = \boldsymbol{\eta}(\boldsymbol{\xi}_1, \boldsymbol{\xi}_2, \mathbf{y}, t)$$
$$\boldsymbol{\xi}_1(t_j^+) = \boldsymbol{\xi}_1(t_j^-), \quad \boldsymbol{\xi}_2(t_j^+) = \boldsymbol{\nu}(\boldsymbol{\xi}_1(t_j), \boldsymbol{\xi}_2(t_j^-), t_j) \tag{6}$$
$$\mathbf{u} = \boldsymbol{\theta}(\boldsymbol{\xi}, t)$$

as that of the plant and with the internal state $\boldsymbol{\xi} = [\boldsymbol{\xi}_1, \boldsymbol{\xi}_2]^\top \in \mathbb{R}^{2s}$, with the time instants $t = t_j$, $j = 1, 2, \ldots$, which are not necessarily coinciding with the collision time instants in the plant equations (1)-(5), and with uniformly bounded in t functions $\boldsymbol{\eta}(\boldsymbol{\xi}, \mathbf{y}, t)$, $\boldsymbol{\nu}(\boldsymbol{\xi}, t)$, and $\boldsymbol{\theta}(\boldsymbol{\xi}, t)$ of class C^1 such that $\boldsymbol{\eta}(\mathbf{0}, \mathbf{0}, t) = \mathbf{0}$, $\boldsymbol{\nu}(\mathbf{0}, t) = \mathbf{0}$, and $\boldsymbol{\theta}(\mathbf{0}, t) = \mathbf{0}$ for all t. Such a controller is said to be a locally *admissible controller* iff the undisturbed closed-loop system (1)-(5), (6) with $\mathbf{w}, \mathbf{w_i^d} = \mathbf{0}$ is uniformly asymptotically stable.

The $\mathcal{H}_\infty$-control problem of interest consists in finding a locally admissible controller (if any) such that the $\mathcal{L}_2$-gain of the disturbed system is less than a certain $\gamma > 0$, that is the inequality

$$\int_{t_0}^{T} \|\mathbf{z}(t)\|^2 \mathrm{d}t + \sum_{i=1}^{N_T} \|\mathbf{z_i^d}\|^2 \leq \gamma^2 \left[\int_{t_0}^{T} \|\mathbf{w}(t)\|^2 \mathrm{d}t + \sum_{i=1}^{N_T} \|\mathbf{w_i^d}\|^2 \right] + \sum_{k=0}^{N_T} \beta_k(\mathbf{x}(t_k^-), \boldsymbol{\xi}(t_k^-), t_k) \tag{7}$$

holds for some positive definite functions $\beta_k(\mathbf{x}, \boldsymbol{\xi}, t)$, $k = 0, \ldots, N_T$, for all segments $[t_0, T]$ and a natural N_T such that $t_{N_T} \leq T < t_{N_T+1}$, for all piecewise continuous disturbances $\mathbf{w}(t)$ and discrete ones $\mathbf{w_i^d}$, $i = 1, 2, \ldots$, for which the state trajectory of the closed-loop system starting from an initial point $(\mathbf{x}(t_0), \boldsymbol{\xi}(t_0)) = (\mathbf{x_0}, \boldsymbol{\xi_0}) \in \mathcal{U}$ remains in some neighborhood $\mathcal{U} \in \mathbb{R}^{2(n+s)}$ of the origin for all $t \in [t_0, T]$.

It is worth noticing that the above $\mathcal{L}_2$-gain definition is consistent with the notion of dissipativity, introduced by ? and ?, and with iISS notion ?, and it represents a natural extension to hybrid systems (see, e.g. the works by ?, ?, ? and ?). In order to facilitate the exposition the underlying system, chosen for treatment, has been pre-specified with the post-impact velocity value $\mathbf{x_2}(t)$ in the discrete output (5) to be controlled. The general case of a certain function $\boldsymbol{\kappa}(\mathbf{x_2}(t))$ of the post impact velocity value in the discrete output (5) can be treated in a similar manner because the $\mathcal{L}_2$-gain inequality (7) is flexible in the choice of positive definite functions $\beta_k(\mathbf{x}, \boldsymbol{\xi}, t)$, $k = 0, \ldots, N_T$.

3.   Output Feedback Synthesis Under Unilateral Constraints

In this section, we present sufficient conditions for the solution of the underlying disturbance attenuation problem to exist. For later use, the continuous dynamics (1) are rewritten in the form

$$\dot{\mathbf{x}} = \mathbf{f}(\mathbf{x}, t) + \mathbf{g_1}(\mathbf{x}, t)\mathbf{w} + \mathbf{g_2}(\mathbf{x}, t)\mathbf{u} \tag{8}$$

whereas the restitution rule is represented as follows

$$\mathbf{x}(t_i^+) = \boldsymbol{\mu}(\mathbf{x}(t_i^-), t_i) + \boldsymbol{\Omega}(\mathbf{x}(t_i^-), t_i)\mathbf{w_i^d}, \ i = 1, 2, \ldots \tag{9}$$

with $\mathbf{x}^\top = [\mathbf{x_1}^\top, \mathbf{x_2}^\top]$, $\mathbf{f}^\top(\mathbf{x}, t) = [\mathbf{x_2}^\top, \boldsymbol{\Phi}^\top(\mathbf{x}, t)]$, $\mathbf{g_1}^\top(\mathbf{x}, t) = [\mathbf{0}, \boldsymbol{\Psi}_1^\top(\mathbf{x}, t)]$, $\mathbf{g_2}^\top(\mathbf{x}, t) = [\mathbf{0}, \boldsymbol{\Psi}_2^\top(\mathbf{x}, t)]$, $\boldsymbol{\mu}^\top(\mathbf{x}, t) = [\mathbf{x_1}^\top, \boldsymbol{\mu}_0^\top(\mathbf{x}, t)]$, and $\boldsymbol{\Omega}^\top(\mathbf{x}, t) = [\mathbf{0}, \boldsymbol{\omega}(\mathbf{x}, t)]$. In order to simplify the synthesis to be

developed and to provide reasonable expressions for the controller design, the standard assumptions

$$\mathbf{h_1}^\top \mathbf{k_{12}} \equiv \mathbf{0}, \quad \mathbf{k_{12}}^\top \mathbf{k_{12}} \equiv \mathbf{I}, \quad \mathbf{k_{21}}\mathbf{g_1}^\top \equiv \mathbf{0}, \quad \mathbf{k_{21}}\mathbf{k_{21}}^\top \equiv \mathbf{I}, \tag{10}$$

are brought from the work of **?** into play. Relaxing these assumptions is indeed possible, but it would substantially complicate the formulas to be worked out.

3.1   *Non-local state-space solution*

Let $B_\delta^{2n} \in \mathbb{R}^{2n}$ be a ball of radius $\delta > 0$, centered around the origin. Given $\gamma > 0$, a solution to the problem in question is derived under the hypotheses, specified below in a domain $(\mathbf{x}, \boldsymbol{\xi}) \in B_\delta^{2n}, t \in \mathbb{R}$ of interest:

H1) the norm of the matrix function $\boldsymbol{\omega}$ is upper bounded by $\frac{\sqrt{2}}{2}\gamma$, i.e.,

$$\|\boldsymbol{\omega}(\mathbf{x}, t)\| \leq \frac{\sqrt{2}}{2}\gamma. \tag{11}$$

H2) there exist a smooth, positive definite, decrescent function $V(\mathbf{x}, t)$ and a positive definite function $R(\mathbf{x})$ such that if computed along the trajectories of the system (1)-(5) with initial conditions within B_δ^{2n}, for all $t \in (t_{i-1}, t_i),\ i = 1, 2, \ldots$ with t_0 being the initial time, and t_i the collision time instants of the disturbed system (1)-(5), the Hamilton–Jacobi–Isaacs inequality

$$\frac{\partial V}{\partial t} + \frac{\partial V}{\partial \mathbf{x}}(\mathbf{f}(\mathbf{x}, t) + \mathbf{g_1}(\mathbf{x}, t)\boldsymbol{\alpha_1} + \mathbf{g_2}(\mathbf{x}, t)\boldsymbol{\alpha_2}) + \mathbf{h_1}^\top \mathbf{h_1} + \boldsymbol{\alpha_2}^\top \boldsymbol{\alpha_2} - \gamma^2 \boldsymbol{\alpha_1}^\top \boldsymbol{\alpha_1} \leq -R(\mathbf{x}) \tag{12}$$

holds with

$$\boldsymbol{\alpha_1}(\mathbf{x}, t) = \frac{1}{2\gamma^2}\mathbf{g}_1^\top(\mathbf{x}, t)\left(\frac{\partial V}{\partial \mathbf{x}}\right)^\top, \quad \boldsymbol{\alpha_2}(\mathbf{x}, t) = -\frac{1}{2}\mathbf{g}_2^\top(\mathbf{x}, t)\left(\frac{\partial V}{\partial \mathbf{x}}\right)^\top;$$

H3) there exist a continuous uniformly bounded function $G(t)$, and a positive semidefinite function $Q(\mathbf{x}, \boldsymbol{\xi})$ subject to $Q(\mathbf{0}, \boldsymbol{\xi})$ which is positive definite, and a smooth, positive semidefinite, decrescent function $W(\mathbf{x}, \boldsymbol{\xi}, t)$ subject to $W(\mathbf{0}, \boldsymbol{\xi}, t)$ which is positive definite, and such that computed along the trajectories of system (1)-(5) with initial conditions within $(\mathbf{x}(t_0), \boldsymbol{\xi}(t_0)) \in B_\delta^{2n}$, for all $t \in (t_{i-1}, t_i)$, the Hamilton-Jacobi-Isaacs inequality

$$\frac{\partial W}{\partial t} + \left(\begin{array}{cc} \frac{\partial W}{\partial \mathbf{x}} & \frac{\partial W}{\partial \boldsymbol{\xi}} \end{array}\right)\mathbf{f_e}(\mathbf{x}, \boldsymbol{\xi}, t) + \mathbf{h_e}^\top \mathbf{h_e} - \gamma^2 \boldsymbol{\psi}^\top \boldsymbol{\psi} \leq -Q(\mathbf{x}, \boldsymbol{\xi}) \tag{13}$$

holds with

$$\mathbf{f_e}(\mathbf{x}, \boldsymbol{\xi}, t) = \left(\begin{array}{c} \mathbf{f}(\mathbf{x}, t) + \mathbf{g_1}(\mathbf{x}, t)\boldsymbol{\alpha_1}(\mathbf{x}, t) + \mathbf{g_2}(\mathbf{x}, t)\boldsymbol{\alpha_2}(\boldsymbol{\xi}, t) \\ \mathbf{f}(\boldsymbol{\xi}, t) + \mathbf{g_1}(\boldsymbol{\xi}, t)\boldsymbol{\alpha_1}(\boldsymbol{\xi}, t) + \mathbf{g_2}(\boldsymbol{\xi}, t)\boldsymbol{\alpha_2}(\boldsymbol{\xi}, t) + \mathbf{G}(t)(\mathbf{h_2}(\mathbf{x}, t) - \mathbf{h_2}(\boldsymbol{\xi}, t)) \end{array}\right)$$

$$\mathbf{h_e}(\mathbf{x}, \boldsymbol{\xi}, t) = \boldsymbol{\alpha_2}(\mathbf{x}, t) - \boldsymbol{\alpha_2}(\boldsymbol{\xi}, t),$$

$$\boldsymbol{\psi}(\mathbf{x}, \boldsymbol{\xi}, t) = \frac{1}{2\gamma^2} \mathbf{g_e}^\top(\mathbf{x}, t) \left(\begin{array}{c} \left(\dfrac{\partial W}{\partial \mathbf{x}} \right)^\top \\[2mm] \left(\dfrac{\partial W}{\partial \boldsymbol{\xi}} \right)^\top \end{array} \right),$$

$$\mathbf{g_e}(\mathbf{x}, t) = \left(\begin{array}{c} \mathbf{g_1}(\mathbf{x}, t) \\ \mathbf{G}(t)\mathbf{k_{21}}(\mathbf{x}, t) \end{array} \right);$$

H4) Hypotheses H2) and H3) are satisfied with the functions $V(\mathbf{x}, t)$ and $W(\mathbf{x}, \boldsymbol{\xi}, t)$ which decrease along the direction $\boldsymbol{\mu}$ in the sense that the inequalities

$$V(\mathbf{x}, t) \geq V(\boldsymbol{\mu}(\mathbf{x}, t), t), \tag{14}$$

$$W(\mathbf{x}, \boldsymbol{\xi}, t) \geq W(\boldsymbol{\mu}(\mathbf{x}, t), \boldsymbol{\mu}(\boldsymbol{\xi}, t), t) \tag{15}$$

hold in the domains of V and W.

The following result is in force.

Theorem 1: *Given $\gamma > 0$, suppose that Hypotheses H1)-H3) are satisfied for system (1)-(5) in a domain $\mathbf{x} \in B_\delta^{2n}, \boldsymbol{\xi} \in B_\delta^{2n}, t \in \mathbb{R}$ with functions $V(x, t)$ and $W(x, \xi, t)$. Then, the closed-loop system (1)-(5), driven by the dynamic controller*

$$\dot{\boldsymbol{\xi}} = \mathbf{f}(\boldsymbol{\xi}, t) + \mathbf{g_1}(\boldsymbol{\xi}, t)\boldsymbol{\alpha_1}(\boldsymbol{\xi}, t) + \mathbf{g_2}(\boldsymbol{\xi}, t)\boldsymbol{\alpha_2}(\boldsymbol{\xi}, t) + \mathbf{G}(t)(\mathbf{y}(\mathbf{x}, t) - \mathbf{h_2}(\boldsymbol{\xi}, t))$$
$$\boldsymbol{\xi_1}(t_i^+) = \boldsymbol{\xi_1}(t_i^-), \ \boldsymbol{\xi_2}(t_i^+) = \boldsymbol{\mu_0}(\boldsymbol{\xi_1}(t_i), \boldsymbol{\xi_2}(t_i^-), t_i) \tag{16}$$
$$\mathbf{u} = \boldsymbol{\alpha_2}(\boldsymbol{\xi}, t),$$

locally possesses a $\mathcal{L}_2$-gain less than γ. Once Hypothesis H4) is satisfied as well, the function

$$U(\mathbf{x}, \boldsymbol{\xi}, t) = V(\mathbf{x}, t) + W(\mathbf{x}, \boldsymbol{\xi}, t) \tag{17}$$

constitutes a Lyapunov function of the disturbance-free closed-loop system (1)-(5), (16) the uniform asymptotic stability of which is thus additionally guaranteed.

3.1.1 Proof of Theorem 1

The proof of Theorem 1 is preceded with an instrumental lemma which extends the powerful Lyapunov approach to impact systems. The following result specifies (**?**, Theorem 2.4) to the present case with $x_1 = x$ and $x_2 = t$.

Lemma 1: *Consider the unforced ($\mathbf{u} = \mathbf{0}$) disturbance-free ($\mathbf{w} = \mathbf{0}$, $\mathbf{w_i^d} = \mathbf{0}$, $i = 1, 2, \ldots$) system (8), (9) with the assumptions above. Let there exist a positive definite decrescent function $V(\mathbf{x}, t)$ such that its time derivative, computed along (8), is negative definite whereas $V(\mathbf{x}, t) \geq V(\boldsymbol{\mu}(\mathbf{x}, t), t)$ for all $t \in \mathbb{R}^1$. Then the system is uniformly asymptotically stable.*

Proof of Theorem 1. Since the proof follows the same line of reasoning as that used in **?** for the impact-free case here we provide only a sketch. Similar to the proof of (**?**, Theorem 7.1), let us differentiate function (17) along the disturbed closed-loop system (1)-(5) and estimate it between

collision time instants (**?**, p.138):

$$\frac{\mathrm{d}U}{\mathrm{d}t} \leq -\|\mathbf{z}(t)\|^2 + \gamma^2\|\mathbf{w}\|^2 - R(\mathbf{x}) - Q(\mathbf{x},\boldsymbol{\xi}) - \gamma^2\|\mathbf{w} - \boldsymbol{\alpha_1}(\mathbf{x},t) - \boldsymbol{\psi}(\mathbf{x},\boldsymbol{\xi},t)\|^2, \tag{18}$$
$$t \in (t_k, t_{k+1}), \quad k = 0, 1, \ldots.$$

Then integrating (18) from t_k to t_{k+1}, $k = 0, 1, \ldots$, yields

$$\int_{t_k}^{t_{k+1}} [\gamma^2\|\mathbf{w}\|^2 - \|\mathbf{z}(t)\|^2]\mathrm{d}t \geq \int_{t_k}^{t_{k+1}} [R(\mathbf{x}(t)) + Q(\mathbf{x}(t),\boldsymbol{\xi}(t))]\mathrm{d}t + \int_{t_k}^{t_{k+1}} \frac{\mathrm{d}U(\mathbf{x}(t),\boldsymbol{\xi}(t),t)}{\mathrm{d}t}\mathrm{d}t$$
$$+\gamma^2\int_{t_k}^{t_{k+1}} \|\mathbf{w}(t) - \boldsymbol{\alpha_1}(\mathbf{x}(t),t) - \boldsymbol{\psi}(\mathbf{x}(t),\boldsymbol{\xi}(t),t)\|^2\mathrm{d}t > 0. \tag{19}$$

Taking (17) into account and skipping positive terms in the right-hand side of (19), it follows that

$$\int_{t_0}^{T} (\gamma^2\|\mathbf{w}\|^2 - \|\mathbf{z}(t)\|^2)\mathrm{d}t \geq U(\mathbf{x}(T),\boldsymbol{\xi}(T),T) + \sum_{i=1}^{N_T}[V(\mathbf{x}(t_i^-),t_i) - V(\mathbf{x}(t_i^+),t_i)]$$
$$+ \sum_{i=1}^{N_T}[W(\mathbf{x}(t_i^-),\boldsymbol{\xi}(t_i^-),t_i) - W(\mathbf{x}(t_i^+),\boldsymbol{\xi}(t_i^+),t_i)] - U(\mathbf{x}(t_0),\boldsymbol{\xi}(t_0),t_0). \tag{20}$$

Since the functions V and W are smooth by Hypotheses H2) and H3) the following relations

$$|V(\mathbf{x}(t_i^-),t_i) - V(\mathbf{x}(t_i^+),t_i)| \leq L_i^V\|\mathbf{x}(t_i^-) - \mathbf{x}(t_i^+)\| \leq L_i^V[\|\mathbf{x}(t_i^-)\| + |\mathbf{x}(t_i^+)\|]$$
$$|W(\mathbf{x}(t_i^-),\boldsymbol{\xi}(t_i^-),t_i) - W(\mathbf{x}(t_i^+),\boldsymbol{\xi}(t_i^-),t_i)| \leq L_i^W[\|\mathbf{x}(t_i^-) - \mathbf{x}(t_i^+)\| + \|\boldsymbol{\xi}(t_i^-) - \boldsymbol{\xi}(t_i^+)\|] \tag{21}$$
$$\leq L_i^W[\|\mathbf{x}(t_i^-)\| + \|\mathbf{x}(t_i^+)\| + \|\boldsymbol{\xi}(t_i^-)\| + \|\boldsymbol{\xi}(t_i^+)\|]$$

hold true with $L_i^V > 0$ and $L_i^W > 0$ being local Lipschitz constants of V and W in the domain $B_\delta^{2n} \in \mathbb{R}^{2n}$. Relations (20) and (21), coupled together, result in the inequality

$$\int_{t_0}^{T} (\gamma^2\|\mathbf{w}\|^2 - \|\mathbf{z}(t)\|^2)\mathrm{d}t \geq -\sum_{i=1}^{N_T}[2(L_i^V + L_i^W)\|\mathbf{x}(t_i^-)\| + 2L_i^W\|\boldsymbol{\xi}(t_i^-)\|] - U(\mathbf{x}(t_0),\boldsymbol{\xi}(t_0),t_0), \tag{22}$$

thus being verified in the domain $B_\delta^{2n} \in \mathbb{R}^{2n}$. Apart from this, inequality

$$\sum_{i=1}^{N_T}\|\mathbf{z_i^d}\|^2 = \sum_{i=1}^{N_T}\|\mathbf{x_2}(t_i^+)\|^2 \leq 2\sum_{i=1}^{N_T}\|\boldsymbol{\mu_0}(\mathbf{x}(t_i^-),t_i)\|^2 + 2\sum_{i=1}^{N_T}\|\boldsymbol{\omega}(\mathbf{x}(t_i^-),t_i)\mathbf{w_i^d}\|^2 \leq$$
$$2\sum_{i=1}^{N_T}\|\boldsymbol{\mu_0}(\mathbf{x}(t_i^-),t_i)\|^2 + \gamma^2\sum_{i=1}^{N_T}\|\mathbf{w_i^d}\|^2 \tag{23}$$

is ensured by Hypothesis H1). Thus, combining (22)-(23), one derives

$$\int_{t_0}^{T} \|\mathbf{z}(t)\|^2 \mathrm{d}t + \sum_{i=1}^{N_T} \|\mathbf{z_i^d}\|^2 \leq U(\mathbf{x}(t_0), \boldsymbol{\xi}(t_0), t_0) + \gamma^2 \left[\int_{t_0}^{T} \|\mathbf{w}(t)\|^2 \mathrm{d}t + \sum_{i=1}^{N_T} \|\mathbf{w_i^d}\|^2 \right] + \tag{24}$$

$$2 \sum_{i=1}^{N_T} \|\boldsymbol{\mu_0}(\mathbf{x}(t_i^-), t_i)\|^2 + \sum_{i=1}^{N_T} [(2L_i^V + 2L_i^W)\|\mathbf{x}(t_i^-)\| + 2L_i^W\|\boldsymbol{\xi}(t_i^-)\|],$$

i.e., the disturbance attenuation inequality (7) is established with the positive definite functions

$$\beta_0(\mathbf{x}(t_0), \boldsymbol{\xi}(t_0), t_0) = U(\mathbf{x}(t_0), \boldsymbol{\xi}(t_0), t_0),$$
$$\beta_i(\mathbf{x}(t_i), \boldsymbol{\xi}(t_i), t_i) = (2L_i^V + 2L_i^W)\|\mathbf{x}(t_i^-)\| + 2L_i^W\|\boldsymbol{\xi}(t_i^-)\| + 2\|\boldsymbol{\mu_0}(\mathbf{x}(t_i^-), t_i)\|^2, \tag{25}$$
$$i = 1, \ldots, N.$$

To complete the proof it remains to establish the asymptotic stability of the undisturbed version of the closed-loop system (1)-(5),(16). Indeed, if coupled to Hypothesis H4), the negative definiteness (18) of the time derivative of the Lyapunov function (17) between the collision time instants, ensures that Lemma 1 is applicable to the undisturbed version of the closed-loop system (1)-(5),(16). By applying Lemma 1, the required asymptotic stability is thus validated. Theorem 1 is proved. ∎

3.2   *Local state-space solution*

To circumvent the difficulty of solving the Hamilton–Jacobi–Isaacs PDIs (12), (13) their solutions are further approximated by those to the corresponding Riccati equations that appear in solving the $\mathcal{H}_\infty$ control problem for the linearized system which is given by

$$\dot{\mathbf{x}} = \mathbf{A}(t)\mathbf{x} + \mathbf{B_1}(t)\mathbf{w} + \mathbf{B_2}(t)\mathbf{u}, \tag{26}$$
$$\mathbf{z} = \mathbf{C_1}(t)\mathbf{x} + \mathbf{D_{12}}(t)\mathbf{u}, \tag{27}$$
$$\mathbf{y} = \mathbf{C_2}(t)\mathbf{x} + \mathbf{D_{21}}(t)\mathbf{w}, \tag{28}$$

within impact-free time intervals (t_{i-1}, t_i) where t_0 is the initial time instant and t_i, $i = 1, 2, \ldots$ are the collision time instants whereas

$$\mathbf{A}(t) = \left. \frac{\partial \mathbf{f}}{\partial \mathbf{x}} \right|_{\mathbf{x=0}}, \ \mathbf{B_1}(t) = \mathbf{g_1}(0, t), \mathbf{B_2}(t) = \mathbf{g_2}(0, t), \ \mathbf{C}(t) = \left. \frac{\partial \mathbf{h}}{\partial \mathbf{x}} \right|_{\mathbf{x=0}}, \ \mathbf{D_{12}}(t) = \mathbf{k_{12}}(0, t). \tag{29}$$

By the time-varying strict bounded real lemma (**?**, p.46), the following conditions are necessary and sufficient for the linear $\mathcal{H}_\infty$ control problem (26)-(28) to possess a solution: given $\gamma > 0$,

C1) there exists a positive constant ε_0 such that the differential Riccati equation

$$-\dot{\mathbf{P}}_\varepsilon(t) = \mathbf{P}_\varepsilon(t)\mathbf{A}(t) + \mathbf{A}^\top(t)\mathbf{P}_\varepsilon(t) + \mathbf{C_1}^\top(t)\mathbf{C_1}(t)$$
$$+\mathbf{P}_\varepsilon(t)[\frac{1}{\gamma^2}\mathbf{B_1}\mathbf{B_1}^\top - \mathbf{B_2}\mathbf{B_2}^\top](t)\mathbf{P}_\varepsilon(t) + \varepsilon\mathbf{I} \tag{30}$$

has a uniformly bounded symmetric positive definite solution $\mathbf{P}_\varepsilon(t)$ for each $\varepsilon \in (0, \varepsilon_0)$;

C2) while being coupled to (30), the differential Riccati equation

$$
\begin{aligned}
\dot{\mathbf{Z}}_\varepsilon(t) = {} & \mathbf{A}_\varepsilon(t)\mathbf{Z}_\varepsilon(t) + \mathbf{Z}_\varepsilon(t)\mathbf{A}_\varepsilon^\top(t) + \mathbf{B_1}(t)\mathbf{B_1}^\top(t) \\
& +\mathbf{Z}_\varepsilon(t)[\frac{1}{\gamma^2}\mathbf{P}_\varepsilon\mathbf{B_2}\mathbf{B_2}^\top\mathbf{P}_\varepsilon - \mathbf{C_2}^\top\mathbf{C_2}](t)\mathbf{Z}_\varepsilon(t) + \varepsilon\mathbf{I},
\end{aligned}
\tag{31}
$$

has a uniformly bounded symmetric positive definite solution $\mathbf{Z}_\varepsilon(t)$ with $\mathbf{A}_\varepsilon(t) = \mathbf{A}(t) + \frac{1}{\gamma^2}\mathbf{B_1}(t)\mathbf{B_1}^\top(t)\mathbf{P}_\varepsilon(t)$.

Next result asserts that these conditions, if coupled to a certain monotonicity condition, are also sufficient for a local solution to the nonlinear $\mathcal{H}_\infty$ control problem to exist under unilateral constraints.

Theorem 2: *Let conditions C1) and C2) be satisfied with some $\gamma > 0$. Then Hypotheses H2) and H3) hold locally around the equilibrium $(\mathbf{x}, \boldsymbol{\xi}) = (0,0)$ of the nonlinear system (1)-(5) with*

$$
V(\mathbf{x}, t) = \mathbf{x}^\top\mathbf{P}_\varepsilon(t)\mathbf{x}
\tag{32}
$$

$$
R(\mathbf{x}) = \frac{\varepsilon}{2}\|\mathbf{x}\|^2
\tag{33}
$$

$$
W(\mathbf{x}, \boldsymbol{\xi}, t) = \gamma^2(\mathbf{x} - \boldsymbol{\xi})^\top\mathbf{Z}_\varepsilon^{-1}(t)(\mathbf{x} - \boldsymbol{\xi})
\tag{34}
$$

$$
Q(\mathbf{x}, \boldsymbol{\xi}) = \frac{\varepsilon}{2}\gamma^2\min_{t\in\mathbb{R}^1}\|\mathbf{Z}_\varepsilon^{-1}(t)\|^2\|\mathbf{x} - \boldsymbol{\xi}\|^2
\tag{35}
$$

$$
G(t) = \mathbf{Z}_\varepsilon(t)\mathbf{C_2}^\top(t)
\tag{36}
$$

and the closed-loop system driven by the output feedback

$$
\begin{aligned}
\dot{\boldsymbol{\xi}} = {} & \mathbf{f}(\boldsymbol{\xi}, t) + \mathbf{G}(t)[\mathbf{y} - \mathbf{h_2}(\boldsymbol{\xi}, t)] + \left[\frac{1}{\gamma^2}\mathbf{g_1}(\boldsymbol{\xi}, t)\mathbf{g_1}^\top(\boldsymbol{\xi}, t) - \mathbf{g_2}(\boldsymbol{\xi}, t)\mathbf{g_2}^\top(\boldsymbol{\xi}, t)\right]\mathbf{P}_\varepsilon(t)\boldsymbol{\xi} \\
& \boldsymbol{\xi_1}(t_i^+) = \boldsymbol{\xi_1}(t_i^-),\ \boldsymbol{\xi_2}(t_i^+) = \boldsymbol{\mu_0}(\boldsymbol{\xi}_1(t_i), \boldsymbol{\xi}_2(t_i^-), t_i) \\
& \mathbf{u} = -\mathbf{g_2}(\boldsymbol{\xi}, t)^\top\mathbf{P}_\varepsilon(t)\boldsymbol{\xi}
\end{aligned}
\tag{37}
$$

locally possesses a $\mathcal{L}_2$-gain less than γ provided that Hypothesis H1 holds as well. Moreover, the disturbance-free closed-loop system (1)-(5), (37) is uniformly asymptotically stable provided that Hypothesis H4) is satisfied with the quadratic functions (32) and (34).

Proof. Due to (**?**, Theorem 24), Hypotheses H2) and H3) locally hold with (32)-(36). Then by applying Theorem 1, the validity of Theorem 2 is concluded.   □

3.3   Remarks on the synthesis of autonomous and periodic systems

For autonomous systems, all functions in (1)-(5) and (26)-(28) are time-independent, and the differential Riccati equations (30) and (31) degenerate to the algebraic Riccati equations with $\dot{\mathbf{P}}_\varepsilon(t) = 0$ and $\dot{\mathbf{Z}}_\varepsilon(t) = 0$. For periodic systems, all functions in (1)-(5) and (26)-(28) are time-periodic, and Theorem 2 admits a time-periodic synthesis (37) which is based on appropriate periodic solutions $\mathbf{P}_\varepsilon(t)$ and $\mathbf{Z}_\varepsilon(t)$ to the periodic differential Riccati equations (30) and (31).

3.4   *State feedback synthesis*

In the full information case where perfect state measurement is available, Theorem 2 is simplified to the static feedback design

$$\mathbf{u} = -\mathbf{g_2}(\mathbf{x}, t)^\top \mathbf{P}_\varepsilon(t)\mathbf{x} \tag{38}$$

and it is summarized as follows.

Theorem 3: *Let Hypothesis H1) and Condition C1) be satisfied with some $\gamma > 0$. Then the closed-loop system driven by the state feedback (38) locally possesses a $\mathcal{L}_2$-gain less than γ. Moreover, the disturbance-free closed-loop system (1)-(5), (38) is uniformly asymptotically stable provided that the function $V(\mathbf{x}, t) = \mathbf{x}^\top \mathbf{P}_\varepsilon(t)\mathbf{x}$ locally satisfies inequality (14).*

The detailed derivation of the state feedback design may be found in (**?**).

4.   Application to Impact Mechanical Systems

The proposed synthesis is now specified for the tracking problem stated for a mechanical manipulator, composed of free-motion phases governed by

$$\mathbf{D}(\mathbf{q})\ddot{\mathbf{q}} + \mathbf{H}(\mathbf{q}, \dot{\mathbf{q}}) = \mathbf{D}_\tau \boldsymbol{\tau} + \mathbf{w_1} \tag{39}$$

beyond a unilateral time-invariant constraint $F_0(\mathbf{q}) = \mathbf{0}$ where

$$F_0(\mathbf{q}) > \mathbf{0}, \tag{40}$$

whereas these free-motion phases are separated by transition phases according to the restitution rule

$$\mathbf{q}(t_i^+) = \mathbf{q}(t_i^-) \tag{41}$$

$$\dot{\mathbf{q}}(t_i^+) = \phi(\mathbf{q}(t_i))\dot{\mathbf{q}}(t_i^-) + \mathbf{w_i^d} \tag{42}$$

when the state trajectory hits the surface

$$F_0(\mathbf{q}(t_i)) = 0, \quad i = 1, 2, \ldots. \tag{43}$$

Hereinafter, $\mathbf{q}, \dot{\mathbf{q}} \in \mathbb{R}^n$ are generalized position and velocity vectors, the control input $\boldsymbol{\tau} \in \mathbb{R}^n$ is a vector of external torques, $\mathbf{w_1} \in \mathbb{R}^n$ is an external disturbance, $\mathbf{w_i^d}$, $i = 1, 2, \ldots$ are discrete perturbations of the velocity restitution rule (42) at *a priori unknown* time instants t_i;, $\phi(\mathbf{q}) \in \mathbb{R}^{n \times n}$ is a position-dependent restitution matrix; $\mathbf{H}(\mathbf{q}, \dot{\mathbf{q}}) \in \mathbb{R}^n$ is the vector of Coriolis, centrifugal and gravitational torques, the inertia matrix $\mathbf{D}(\mathbf{q})$ and the actuation matrix $\mathbf{D}_\tau$ are of appropriate dimensions such that $\mathbf{D}(\mathbf{q})$ is symmetric and positive definite, and $\mathbf{D}_\tau$ is invertible and is composed of zero and unit values (thus considering only fully actuated mechanical systems); the scalar function $F_0(\mathbf{q})$ relies on the unilateral constraint, imposed on the robot. As a matter of fact, $\mathbf{D}(\mathbf{q})$, and $\mathbf{H}(\mathbf{q}, \dot{\mathbf{q}})$, and $\phi(\mathbf{q})$ are smooth functions in their arguments.

In what follows, the research is confined to the tracking control problem where the output to be controlled is given in terms of the state deviation from a reference trajectory $\mathbf{q^r}(t)$ and it is

composed of the continuous time component

$$
\mathbf{z} = \begin{bmatrix} \mathbf{0} \\ \rho_p(\mathbf{q} - \mathbf{q^r}) \\ \rho_v(\dot{\mathbf{q}} - \dot{\mathbf{q}}^{\mathbf{r}}) \end{bmatrix} + \begin{bmatrix} \mathbf{1} \\ \mathbf{0} \\ \mathbf{0} \end{bmatrix} \mathbf{u}
\tag{44}
$$

with positive weight coefficients ρ_p, ρ_v, and its discrete counterpart

$$
\mathbf{z_i^d} = \dot{\mathbf{q}}(t_i^+) - \dot{\mathbf{q}}^{\mathbf{r}}(t_i^+)
\tag{45}
$$

whereas the available measurement

$$
\mathbf{y} = \mathbf{q} - \mathbf{q^r} + \mathbf{w_0}
\tag{46}
$$

is affected by the measurement error $\mathbf{w_0}(t)$. In order to respect (10) the output to be controlled has been pre-specified in the form (44) where the zero symbols and unit ones stand for zero and identity matrix entries of appropriate dimensions.

The reference trajectory $\mathbf{q^r}(t)$ to be tracked is a periodic trajectory subject to an impact that occurs when the reference trajectory achieves the surface $F_0(\mathbf{q^r}) = 0$. The restitution law during this impact phase is given by

$$
\dot{\mathbf{q}}^{\mathbf{r}}(t_i^+) = \phi(\mathbf{q^r}(t_i))\dot{\mathbf{q}}^{\mathbf{r}}(t_i^-), \quad i = 1, 2, \ldots.
\tag{47}
$$

This trajectory may be constructed off-line with *a priori* known impact instants t_i, $i = 1, 2, \ldots$.

4.1 *Hybrid Error Dynamics*

Let us now introduce the state deviation vector $\mathbf{x} = (\mathbf{x_1}, \mathbf{x_2})^\top$ where $\mathbf{x}_1(t) = \mathbf{q}(t) - \mathbf{q^r}(t)$ and $\mathbf{x}_2(t) = \dot{\mathbf{q}}(t) - \dot{\mathbf{q}}^{\mathbf{r}}(t)$. Then, rewriting the state equations (39)-(43),(44)-(46) in terms of the errors $\mathbf{x_1}$ and $\mathbf{x_2}$ yields the continuous dynamics

$$
\begin{aligned}
\dot{\mathbf{x}}_1 &= \mathbf{x_2} \\
\dot{\mathbf{x}}_2 &= \mathbf{D^{-1}}(\mathbf{x_1} + \mathbf{q^r})[-\mathbf{H}(\mathbf{x_1} + \mathbf{q^r}, \mathbf{x_2} + \dot{\mathbf{q}}^{\mathbf{r}}) + \mathbf{D_\tau}\boldsymbol{\tau} + \mathbf{w_1}] - \ddot{\mathbf{q}}^{\mathbf{r}}
\end{aligned}
\tag{48}
$$

of the error system.

The transitions occur in the error dynamics according to the following scenarios.

T1) The reference trajectory reaches its predefined impact time instant $t = t^k$, $k = 1, 2, \ldots$ when it hits the unilateral constraint whereas the plant remains beyond this constraint, i.e., $F_0(\mathbf{q^r}(t^k)) = 0$, $F_0(\mathbf{x_1}(t^k) + \mathbf{q^r}(t^k)) \neq 0$;

T2) The plant hits the unilateral constraint at $t = t^j$, $j = 1, 2, \ldots$ while the reference trajectory is beyond this constraint, i.e., $F_0(\mathbf{q^r}(t^j)) \neq 0$, $F_0(\mathbf{x_1}(t^j) + \mathbf{q^r}(t^j)) = 0$;

T3) Both the reference trajectory and the plant hits the unilateral constraint at the same time instant $t = t^l$, $l = 1, 2, \ldots$ (what can deliberately be enforced by modifying the pre-specified reference trajectory on-line), i.e., $F_0(\mathbf{q^r}(t^l)) = 0$, $F_0(\mathbf{x_1}(t^l) + \mathbf{q^r}(t^l)) = 0$.

Transition errors are then represented as follows.

Scenario T1:

$$
\begin{aligned}
\mathbf{x_1}(t^{k+}) &= \mathbf{x_1}(t^{k-}) \\
\mathbf{x_2}(t^{k+}) &= \boldsymbol{\mu}^1(\mathbf{x}(t^{k-}), t^k) + \mathbf{w_k^d},
\end{aligned}
\tag{49}
$$

provided that $F_0(\mathbf{q^r}(t^k)) = 0$ and $F_0(\mathbf{x_1}(t^k) + \mathbf{q^r}(t^k)) \neq 0, \; k = 1, 2, \ldots;$

Scenario T2:

$$
\begin{aligned}
\mathbf{x_1}(t^{j+}) &= \mathbf{x_1}(t^{j-}) \\
\mathbf{x_2}(t^{j+}) &= \boldsymbol{\mu}^2(\mathbf{x}(t^{j-}), t^j) + \mathbf{w_j^d},
\end{aligned}
\tag{50}
$$

provided that $F_0(\mathbf{q^r}(t^j)) \neq 0$ and $F_0(\mathbf{x_1}(t^j) + \mathbf{q^r}(t^j)) = 0, \; j = 1, 2, \ldots;$

Scenario T3:

$$
\begin{aligned}
\mathbf{x_1}(t^{l+}) &= \mathbf{x_1}(t^{l-}) \\
\mathbf{x_2}(t^{l+}) &= \boldsymbol{\mu}^3(\mathbf{x}(t^{l-}), t^l) + \mathbf{w_l^d}, \; l = 1, 2, \ldots
\end{aligned}
\tag{51}
$$

provided that $F_0(\mathbf{q^r}(t^l)) = 0$ and $F_0(\mathbf{x_1}(t^l) + \mathbf{q^r}(t^l)) = 0, \; l = 1, 2, \ldots$

where $\mathbf{w_k^d}$, $\mathbf{w_j^d}$, $\mathbf{w_l^d}$ are discrete perturbations, counting for restitution inadequacies, and functions $\boldsymbol{\mu}^1$, $\boldsymbol{\mu}^2$, and $\boldsymbol{\mu}^3$ are given by

$$
\boldsymbol{\mu}^1(\mathbf{x}, t) = \mathbf{x_2} + [\mathbf{I} - \phi(\mathbf{q^r}(t))]\dot{\mathbf{q}}^r(t^-)
\tag{52}
$$

$$
\boldsymbol{\mu}^2(\mathbf{x}, t) = \phi(\mathbf{x_1} + \mathbf{q^r}(t))[\mathbf{x_2} + \dot{\mathbf{q}}^r(t^-)] - \dot{\mathbf{q}}^r(t^-)
\tag{53}
$$

$$
\boldsymbol{\mu}^3(\mathbf{x}, t) = \phi(\mathbf{x_1} + \mathbf{q^r}(t)[\mathbf{x_2} + \dot{\mathbf{q}}^r(t^-)] - \phi(\mathbf{q^r}(t))\dot{\mathbf{q}}^r(t^-).
\tag{54}
$$

In order to put the previous equations into the form (4), it suffices to set

$$
F(\mathbf{x}, t) = F_0(\mathbf{x_1} + \mathbf{q^r}(t)), \quad \boldsymbol{\omega}(\mathbf{x}, t) = \mathbf{I}
\tag{55}
$$

and specify the function $\boldsymbol{\mu_0}(\mathbf{x}, t)$ by means of

$$
\boldsymbol{\mu_0}(\mathbf{x}, t) = \left\{
\begin{array}{ll}
\boldsymbol{\mu}^1(\mathbf{x}, t) & \text{if } F_0(\mathbf{q^r}(t)) = 0, \quad F_0(\mathbf{x_1} + \mathbf{q^r}) \neq 0 \\
\boldsymbol{\mu}^2(\mathbf{x}, t) & \text{if } F_0(\mathbf{q^r}(t)) \neq 0, \quad F_0(\mathbf{x_1} + \mathbf{q^r}) = 0 \\
\boldsymbol{\mu}^3(\mathbf{x}, t) & \text{if } F_0(\mathbf{q^r}(t)) = 0, \quad F_0(\mathbf{x_1} + \mathbf{q^r}) = 0.
\end{array}
\right.
\tag{56}
$$

Clearly, the functions $\boldsymbol{\mu_0}(\mathbf{x}, t), \boldsymbol{\omega}(\mathbf{x}, t), F(\mathbf{x}, t)$, thus specified, meet the assumptions, imposed on the generic system (1)-(5) to be twice continuously differentiable in the state domain for all t and to be piece-wise continuous and uniformly bounded in t for all state variables $\mathbf{x}$ in some neighborhood around the origin.

4.2 Pre-Feedback Design and Controller Synthesis

In the case where only the generalized positions of the mechanical system are available for measurements, the pre-feedback design

$$
\boldsymbol{\tau} = \mathbf{D_\tau}^{-1}[\mathbf{D}(\mathbf{q^r})\ddot{\mathbf{q}}^r + \mathbf{H}(\mathbf{q^r}, \dot{\mathbf{q}}^r) + \mathbf{u}]
\tag{57}
$$

computes the Coriolis, centrifugal and gravitational torques on the reference trajectories rather than those occurring in the plant. Thus, the position feedback controller to be constructed consists of a disturbance attenuator $\mathbf{u}$, internally stabilizing the biped around the desired trajectory, and the remainder, which is responsible for the compensation of the reference trajectory and the torques, associated with this trajectory.

Substituting the position pre-feedback (**??**) into (48) yields the impact-free error dynamics in the form

$$\dot{\mathbf{x}}_1 = \mathbf{x}_2$$
$$\dot{\mathbf{x}}_2 = \mathbf{D}^{-1}(\mathbf{x}_1 + \mathbf{q}^{\mathbf{r}})[-\mathbf{H}(\mathbf{x}_1 + \mathbf{q}^{\mathbf{r}}, \mathbf{x}_2 + \dot{\mathbf{q}}^{\mathbf{r}}) + \mathbf{D}(\mathbf{q}^{\mathbf{r}})\ddot{\mathbf{q}}^{\mathbf{r}} + \mathbf{H}(\mathbf{q}^{\mathbf{r}}, \dot{\mathbf{q}}^{\mathbf{r}}) + \mathbf{u} + \mathbf{w}_1] - \ddot{\mathbf{q}}^{\mathbf{r}}$$

(58)

These error dynamics represent a particular form of the generic system (2)-(3), (8)-(9), when specified with (**??**)-(**??**) and

$$\mathbf{f}(\mathbf{x}, t) = \begin{bmatrix} \mathbf{x}_2 \\ \mathbf{D}^{-1}(\mathbf{x}_1 + \mathbf{q}^{\mathbf{r}})[-\mathbf{H}(\mathbf{x}_1 + \mathbf{q}^{\mathbf{r}}, \mathbf{x}_2 + \dot{\mathbf{q}}^{\mathbf{r}}) + \mathbf{D}(\mathbf{q}^{\mathbf{r}})\ddot{\mathbf{q}}^{\mathbf{r}} + \mathbf{H}(\mathbf{q}^{\mathbf{r}}, \dot{\mathbf{q}}^{\mathbf{r}})] - \ddot{\mathbf{q}}^{\mathbf{r}} \end{bmatrix}$$

$$\mathbf{g}_1(\mathbf{x}, t) = \begin{bmatrix} \mathbf{0} & \mathbf{0} \\ \mathbf{0} & \mathbf{D}^{-1}(\mathbf{x}_1 + \mathbf{q}^{\mathbf{r}}) \end{bmatrix}, \quad \mathbf{h}_1(\mathbf{x}) = \begin{bmatrix} \mathbf{0} \\ \rho_p \mathbf{x}_1 \\ \rho_v \mathbf{x}_2 \end{bmatrix},$$

$$\mathbf{g}_2(\mathbf{x}, t) = \begin{bmatrix} \mathbf{0} \\ \mathbf{D}^{-1}(\mathbf{x}_1 + \mathbf{q}^{\mathbf{r}}) \end{bmatrix}, \quad \mathbf{k}_{12}(\mathbf{x}) = \begin{bmatrix} \mathbf{1} \\ \mathbf{0} \\ \mathbf{0} \end{bmatrix}$$

$$\mathbf{h}_2(\mathbf{x}) = \begin{bmatrix} \mathbf{x}_1 & \mathbf{0} \end{bmatrix}, \quad \mathbf{k}_{21}(\mathbf{x}) = \begin{bmatrix} \mathbf{1} & \mathbf{0} \end{bmatrix}, \quad \mathbf{w} = [\mathbf{w}_0^\top \mathbf{w}_1^\top]^\top. \tag{59}$$

Theorem 2, which is straightforwardly applicable to the generic system (2)-(3), (8)-(9), specified with (**??**)-(**??**) and (**??**), constitutes the desired $\mathcal{H}_\infty$-position feedback tracking of the mechanical manipulator under the unilateral constraints. Theorem 3, applied to the same error system, constitutes the $\mathcal{H}_\infty$-tracking synthesis using state feedback.

5. Illustrative Example: Regulation and Orbital Stabilization under Unilateral Constraints

The objective of this section is to illustrate the effectiveness of the developed synthesis with a simple example that captures all the essential features of the general treatment under unilateral constraints.

5.1 *MSDB model*

A simple testbed of interest is depicted in Fig. **??** where m represents the mass, k the spring constant, b the damping constant, τ is the applied control force, and q represents the position. For the free-motion dynamics ($q > 0$), the plant equation reads

$$\ddot{q} = -\frac{k}{m}q - \frac{b}{m}\dot{q} + \frac{1}{m}\tau + \frac{1}{m}w_1 \tag{60}$$

whereas for the transition phase $(q = 0)$, the restitution rule is given by

$$q^+ = q^-, \quad \dot{q}^+ = -e\dot{q}^- + w_i^d, \quad e \in [0, 1]. \tag{61}$$

For brevity, the notation q^+ (q^-) stands for the post-impact (pre-impact) values $q(t_i^+)$ $(q(t_i^-))$ at impact instants t_1, $i = 1, 2, \ldots$. The variables w_1 and w_i^d are introduced to account for non-modeled external forces and model inadequacies such as friction and restitution uncertainties.

In order to address position feedback tracking of a reference trajectory $q^r(t)$, the state error variables

$$x_1 = q - q^r, \ x_2 = \dot{q} - \dot{q}^r \tag{62}$$

and the position measurement

$$y = x_1 + w_0 \tag{63}$$

are involved where w_0 stands for the measurement noise. Inspired from (**??**), the pre-feedback control law

$$\tau = m\ddot{q}^r + b\dot{q}^r + kq^r + u, \tag{64}$$

is composed of a controller u to be designed and the rest being a trajectory compensator. Then, setting $\mathbf{x} = (x_1, x_2)^\top$, $\mathbf{w} = (w_0, w_1)^\top$, and rewriting the system (**??**)-(**??**) in terms of the tracking error variables, one derives

free-motion phase error dynamics

$$\dot{\mathbf{x}} = \underbrace{\begin{bmatrix} 0 & 1 \\ -\frac{k}{m} & -\frac{b}{m} \end{bmatrix}}_{\mathbf{A}} \mathbf{x} + \underbrace{\begin{bmatrix} 0 & 0 \\ 0 & \frac{1}{m} \end{bmatrix}}_{\mathbf{B_1}} \mathbf{w} + \underbrace{\begin{bmatrix} 0 \\ \frac{1}{m} \end{bmatrix}}_{\mathbf{B_2}} u \tag{65}$$

within the constraint $F_0(\mathbf{x}, t) = x_1 + q^r(t) > 0$ and

transition phase error system

$$\mathbf{x}^+ = \begin{bmatrix} x_1^- \\ \mu_0(\mathbf{x}, t) \end{bmatrix} + \begin{bmatrix} 0 \\ 1 \end{bmatrix} w_i^d. \tag{66}$$

on the constraint surface $F_0(\mathbf{x}, t) = x_1 + q^r(t) = 0$ where

$$\mu_0(\mathbf{x}, t) = \begin{cases} x_2 + (1 + e)\dot{q}^r & \text{if } F_0(q^r(t)) = 0, \ F_0(x_1 + q^r) \neq 0 \\ -e(x_2 + \dot{q}^r) - \dot{q}^r & \text{if } F_0(q^r(t)) \neq 0, \ F_0(x_1 + q^r) = 0 \\ -ex_2 & \text{if } F_0(q^r(t)) = 0, \ F_0(x_1 + q^r) = 0, \end{cases} \tag{67}$$

is obtained by specifying (47)-(**??**) to the present case.

In terms of the tracking errors, the variables to be controlled are specified in the form

$$\mathbf{z} = \underbrace{\begin{bmatrix} 0 & 0 \\ \rho_p & 0 \\ 0 & \rho_v \end{bmatrix}}_{\mathbf{C_1}} \mathbf{x} + \underbrace{\begin{bmatrix} 1 \\ 0 \\ 0 \end{bmatrix}}_{\mathbf{D_{12}}} u \tag{68}$$
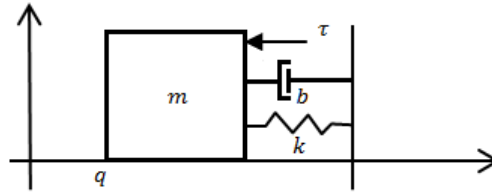
$$z_i^d = -ex_2^- + w_i^d, \tag{69}$$

Figure 1.: Mass-Spring-Damper-Barrier (MSDB) system

complying with (10).

5.2 State Feedback Regulation

To begin with, the tracking of the MSDB system is treated in a particular case under the perfect knowledge of the state vector $\mathbf{q} = (q, \dot{q})^\top$ with the trivial reference trajectory degenerated to the origin $q^r = 0$, $\dot{q}^r = 0$, $\ddot{q}^r = 0$ while the pre-feedback (??) is simplified to the form $\tau = u$ with no trajectory compensation. Just in case, the robust regulation to the origin is synthesized according to Theorem 3, the applicability of which to the MSDB error system (??)-(??) is verified as follows.

To verify condition C1), the generic time-invariant terms $\mathbf{A}$, $\mathbf{B_1}$, $\mathbf{B_2}$, $\mathbf{C_1}$ in the Riccati equation (30) are specified from (??)-(??). A constant positive semidefinite solution of the corresponding time-invariant equation (30) subject to $\varepsilon = 0$ is then obtained by iterating on γ in order to approach the infimal achievable level $\gamma_{min} \approx 1.01$. The value $\gamma = 2$ is subsequently selected to avoid an undesired high-gain controller design that would appear for a value of γ close to the infimal $\gamma_{min} \approx 1.01$. With $\gamma = 2$, the value $\varepsilon = 0.01$ is obtained so that the corresponding perturbed Riccati equation (30) possesses a constant positive definite solution, given by

$$\mathbf{P}_\varepsilon = \begin{bmatrix} 4.9542 & 0.0504 \\ 0.0504 & 4.9542 \end{bmatrix}. \tag{70}$$

Inequality (11) of Hypothesis H1) is straightforwardly verified for $\omega = 1$ and for the corresponding value $\gamma = 2$.

Finally, it remains to verify the last condition (14) of Theorem 3. For this purpose, it suffices to note that only scenario T3) is in force for the state feedback regulation, and therefore in the disturbance-free case, $x_2^+ = -ex_2^-$ by virtue of (??), and hence $\|\mathbf{x}^+\| \leq \|\mathbf{x}^-\|$ for an admissible restitution parameter $e \in [0, 1]$. Thus, Theorem 3, constituting the robust state feedback synthesis under unilateral constraints, becomes applicable to the stabilization of the MSDB system around the origin, and function $V(\mathbf{x}, t) = \mathbf{x}^\top \mathbf{P}_\varepsilon \mathbf{x}$, specified with (??), is a Lyapunov function for the undisturbed system.

5.2.1 Numerical Results

The performance of the closed-loop system, driven by the controller, designed according to Theorem 3, is numerically illustrated in the sequel. The parameters, used in the simulation, are presented in Table ??.

¿From Fig. ??a that depicts the disturbance-free regulation errors, escaping to zero, one concludes that the MSDB system is actually regulated to the barrier. The monotonically decreasing evolution (between and across the impacts) of the quadratic Lyapunov function (32), specified with the Riccati matrix (??), is presented in Fig. ??b. Figure ??a shows that while the disturbing friction force w_1 and deviation w_i^d in the restitution coefficient are added to MSDB testbed (see Table ?? for their numerical values) these disturbances are actually attenuated by the controller designed.

Table 1.: Simulation parameters

Param	Value	Param	Value
k	$10\ N/m$	ρ_v	1
b	$1\ N/m/s$	ε	0.01
m	$1\ kg$	w_i^d	$0.2q_2\ m/s$
e	0.5	w_1	$0.1q_2 + 0.1\text{sign}(q_2)\ N$
ρ_p	1	$q(0)$	$0.5\ m$
$\dot{q}(0)$	$-0.2\ m/s$	$-$	$-$

(a)   (b)
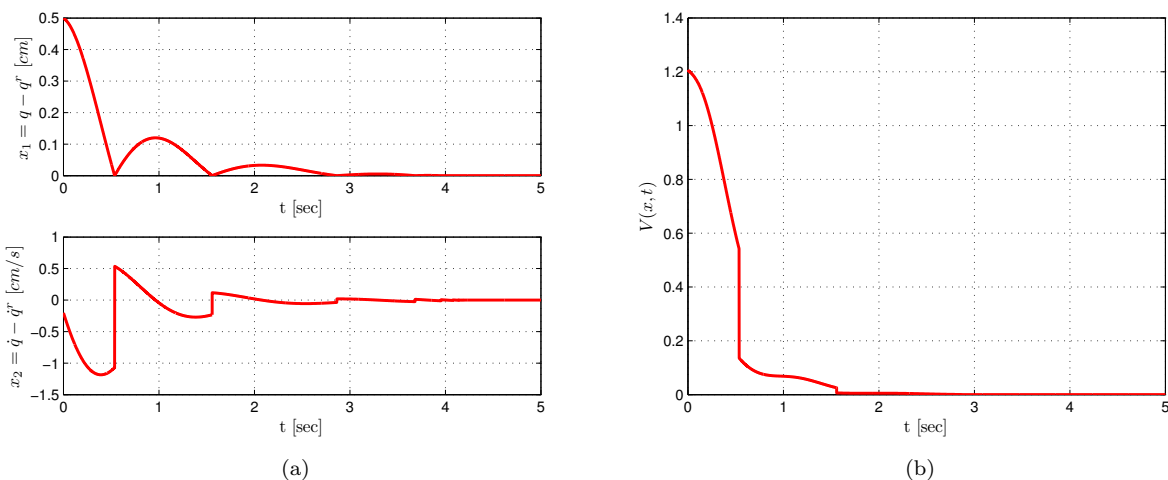
Figure 2.: Numerical results for the disturbance free case of regulation problem. a) Position and velocity errors. b) Lyapunov function evolution.

In addition, Fig. **??**b demonstrates that the output of the system remains bounded to match the $\mathcal{L}_2$-gain inequality (7).

5.3 *Position Feedback Tracking*

In the remainder, the $\mathcal{H}_\infty$-orbitally stabilizing output feedback synthesis is developed using a hybrid version of the Van der Pol oscillator, generating a stable limit cycle to follow.

5.3.1 *Periodic Trajectory Generation*

In the present study, the periodic trajectory to follow is generated by a Van der Pol oscillator subject to an unilateral constraint:

Free-motion phase $(q^r > 0)$

$$\ddot{q}^r = q^r - (1 - q^{r2})\dot{q}^r \tag{71}$$

Transition phase $(q^r = 0)$

$$q^r(t_i^+) = q^r(t_i^-), \quad \dot{q}^r(t_i^+) = -e\dot{q}^r(t_i^-) \tag{72}$$

where q^r represents the desired position and $\dot{q}^r$ the velocity, $t_i,\ i = 1, 2, \ldots$ are impact instants when the oscillator hits the constraint $q^r = 0$.

It is well-known (**?**) that such an impact oscillator is capable of generating a discontinuous limit cycle. In what follows, the restitution parameter is set to $e = 0.5$, and the method of Poincaré
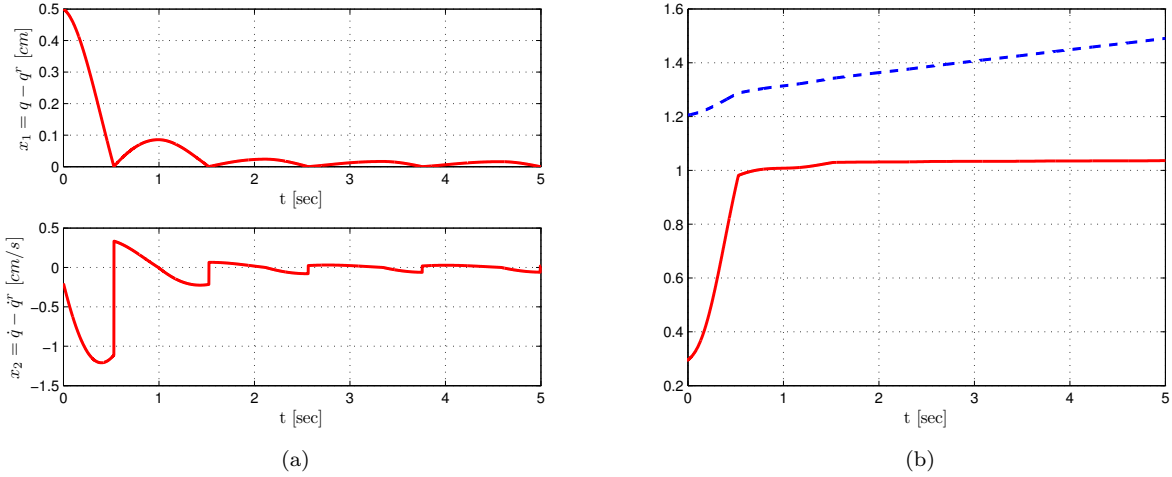
Figure 3.: Numerical results for the disturbed case of regulation problem. a) Position and velocity errors. b) $\mathcal{L}_2$-gain behavior for $\gamma = 2$: $\|z\|_{L_2}^2 + \|z^d\|_{l_2}^2$ (solid line) versus $\gamma^2[\|w\|_{L_2}^2 + \|w_i^d\|_{l_2}^2] + \Sigma_{k=0}^N \beta_k$ (dashed line).

sections is used to ensure that the impact reference model (??)-(??) possesses a stable limit cycle. The Poincaré map Γ, associated with the Poincaré section $q^r = 0$, is given by

$$\Gamma(\mathbf{q}_k^r) = \mathbf{q}_{k+1}^r \tag{73}$$

in terms of the post-impact values $\mathbf{q}_k^r = [q_k^r, \dot{q}_k^r]$ of the solution of the nonlinear differential equation (??) subject to the velocity restitution (??) at the impact instants t_k, $k = 1, 2, \ldots$. Since it is hardly possible to design this map analytically a step-by-step numerical integration of (??)- (??) is subsequently involved. Taking into account that the position component of the state vector remains zero on the Poincaré section $q^r = 0$ only the evolution of the velocity component along the Poincaré section, thus specified, is of interest. With this in mind, Fig. ?? depicts the projection of the Poincaré map (??) onto the velocity subspace where $\dot{q}_{k+1}^r$ is computed as a function of $\dot{q}_k^r$ by numerical integration of (??)-(??) initialized on the Poincaré section $q^r = 0$ with the velocity $\dot{q}_k^r$.

A fixed point $\mathbf{q}^{r^*}$ of the the Poincaré map (??) is determined by the relation

$$\mathbf{q}^{r^*} = \Gamma(\mathbf{q}^{r^*}). \tag{74}$$

and it is located in the intersection of the Poincaré map with the identity map (see Fig. ??). Solving the fixed point equation (??) numerically yields $\mathbf{q}^{r^*} = [0, 1.012]^\top$.

In order to demonstrate that this fixed point is locally asymptotically stable, the eigenvalues of the gradient $\nabla\Gamma$ of the Poincaré map (??) are numerically computed

$$eig(\nabla\Gamma) = [0, -0.224]^\top,$$

thus making sure that both eigenvalues are inside the unity circle. Hence (?, Section 5), the fixed point $\mathbf{q}^{r^*}$ is locally asymptotically stable. By applying (?, Theorem 1), it follows that the locally asymptotically stable fixed point $\mathbf{q}^{r^*}$ of the Poincaré map (??) generates an asymptotically stable limit cycle of hybrid Van der Pol oscillator (??)-(??), which is depicted in Fig. ??.
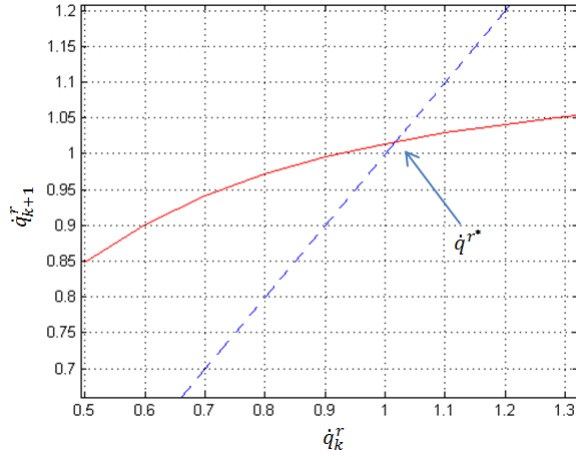
18

Figure 4.: Cobweb plot of the post-impact velocity. The solid line represents the Poincaré map projection on the velocity subspace and the dashed line represents the identity map. The arrows represent the evolution from a random starting point.
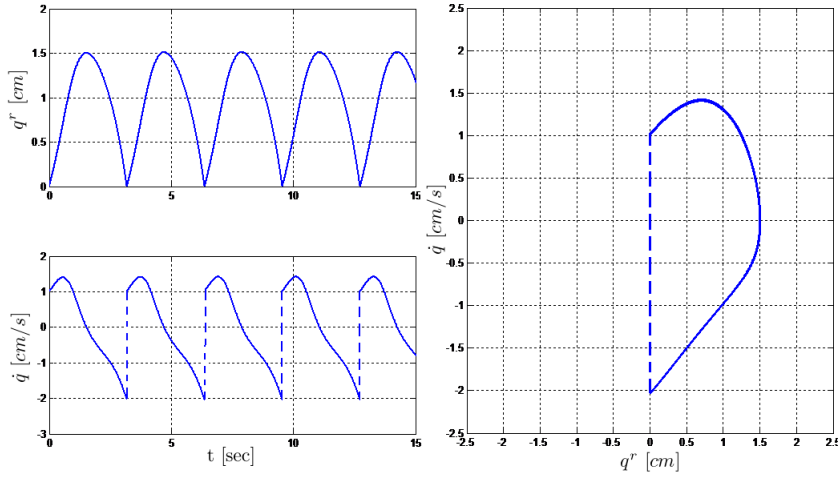

Figure 5.: Evolutions of the position $q^r(t)$ and velocity $\dot{q}^r(t)$ of the impact Van der Pol oscillator (**??**)-(**??**): the vertical dashed lines are for jumps in $\dot{q}^r$ when a resetting event occurs.

5.3.2   Controller Synthesis

The position feedback synthesis is based on Theorem 2, which is now applied to the error dynamics (**??**), (**??**)-(**??**), driven by (**??**), to ensure robust tracking of the desired trajectory, governed by (**??**)-(**??**). By substituting the right-hand side of (**??**) into (**??**) for $\ddot{q}^r$, the pre-feedback controller (**??**), fed by the output of the impact Van der Pol reference model (**??**)-(**??**), is represented in the form

$$\tau = -m[(1 - q^{r2})\dot{q}^r - q^r] + b\dot{q}^r + kq^r + u. \tag{75}$$

As to the error restitution rule, it is actually given by (**??**).

The applicability of Theorem 2 to the present case is verified as follows. Similar to the regulation case, conditions C1) and C2) are verified with the linearizing terms $\mathbf{A}$, $\mathbf{B_1}$, $\mathbf{B_2}$, $\mathbf{C_1}$, $\mathbf{C_2}$, which are required to specify the Riccati equations (30)-(31) and which are identified from (**??**)-(**??**), (**??**). A constant positive semidefinite solution of the corresponding time-invariant system (30)-(31) subject to $\varepsilon = 0$ is then derived for sufficiently large γ and by iterating on γ the infimal achievable level

19

Table 2.: Simulation parameters

Param	Value	Param	Value
$q(0)$	$0.5\ m$	$\dot{q}(0)$	$-0.2\ m/s$
$\xi_1(0)$	$0.1\ m$	$\xi_2(0)$	$0.2\ m/s$
w_2	$0.1\sin(1.5t)\ m$	-	-

$\gamma_{min} \approx 1.01$ is approached. The value $\gamma = 2$ was however selected to avoid an undesirable high-gain controller design which would appear for a value of γ close to the optimum $\gamma_{min} \approx 1.01$. With $\gamma = 2$, the corresponding perturbed Riccati equations (30)-(31) are carried out to possess constant positive definite solutions

$$\mathbf{P}_\varepsilon = \left[\begin{array}{cc} 4.9542 & 0.0504 \\ 0.0504 & 4.9542 \end{array} \right], \quad \mathbf{Z}_\varepsilon = \left[\begin{array}{cc} 0.0715 & -0.0024 \\ -0.0024 & 0.7107 \end{array} \right]. \tag{76}$$

under the value $\varepsilon = 0.01$ which is obtained by iterating on ε.

After that, the value $\gamma = 2$ is straightforwardly verified to meet Hypothesis H1) with $\omega = 1$, corresponding to the present investigation. Thus, Theorem 2 ensures that the underlying closed-loop system possesses $\mathcal{L}_2$-gain less than $\gamma = 2$.

Since the impact instants of the reference trajectory are not in general synchronized with the plant impact instants (unless the reference initial state coincides with that of the plant), whichever scenario T1)-T3) may occur according to the adopted state error restitution rule (**??**). Therefore, Hypothesis H4) is ruled out by the resulting synthesis which proves to be incapable to asymptotically stabilize the closed-loop system even in the disturbance-free case as is well-known from **?**. Nevertheless, the proposed controller does attenuate external/restitution disturbances and measurement noise as established by Theorem 2 before, and while being numerically tested, the performance of the closed-loop system is observed to be acceptable.

5.3.3   Numerical results

The simulation results, shown in Figs. **??-??**, were performed under the same circumstances of Section **??**, using the parameters from Table **??** and additional parameters from Table **??**. The disturbance-free case is presented in Figs. **??-??**. These figures exhibit peaking phenomena since the plant velocity jumps do not match the reference velocity jumps (as clearly observed in Fig. **??**), thus falling into either Scenario T1 or T2 of Section 4.1. The Lyapunov candidate function (17), specified with (32), (34), and (**??**), is thus monotonically decreasing just between impacts while exhibiting undesired increments at the impact time instants (see Fig. **??**), and the asymptotic stability proof is no longer applicable to the disturbance-free case under both Scenarios T1 and T2. Despite the discrepancy in the impact instants of the plant velocity and of the reference velocity, the $\mathcal{L}_2$-gain inequality (7) is still guaranteed by Theorem 2, and good behavior of the closed-loop system with the tracking errors, approaching zero between the impact instants, is concluded from Fig. **??** in the disturbance-free case. From Figs. **??** and **??**, good performance is also concluded for the periodic tracking synthesis despite the added disturbances, affecting the free-motion (due to friction) and transition phases (due to uncertainty in the restitution coefficient).

Finally, the estimated velocity $\dot{q}_{obs} = \xi_2 + \dot{q}^r$ and the observation error $x_{2obs} := x_2 - \xi_2$ are compared in Figs. **??** and **??** for the disturbed and undisturbed cases, respectively. One can observe that if disturbances are not applied, the filter adequately tracks the system velocity between the impact times (Fig. **??**), whereas a reasonably small observation error persists in the disturbed case (Fig. **??**), such that good tracking performance is achieved.
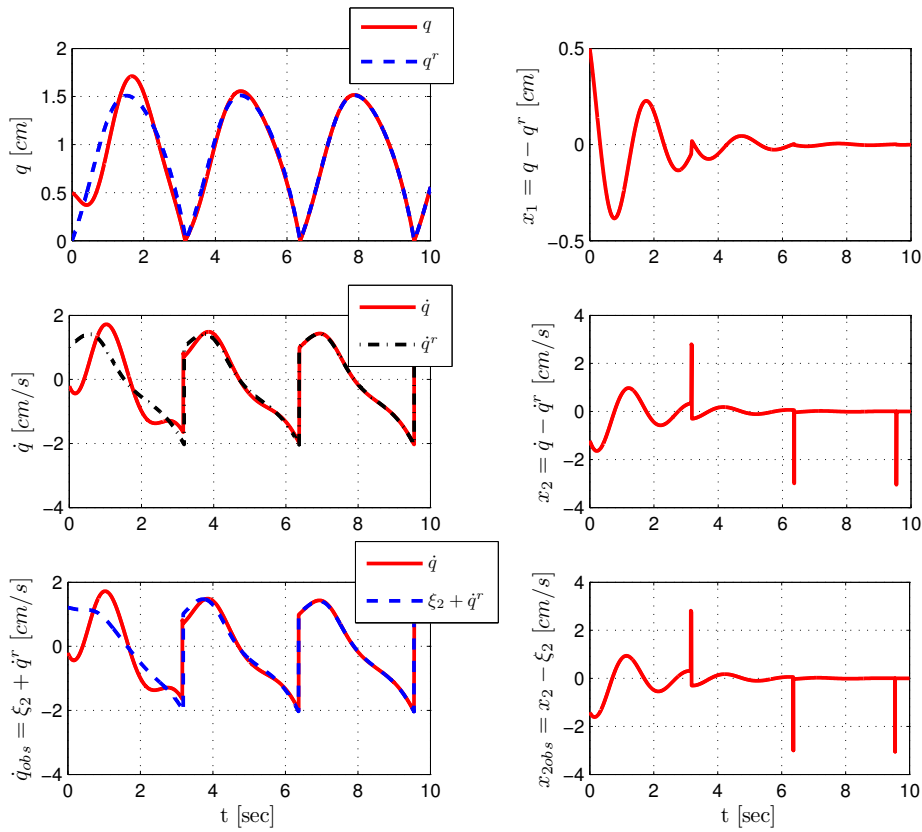
Figure 6.: Plots of the position and velocity tracking errors, and of velocity estimation error in the disturbance-free case.
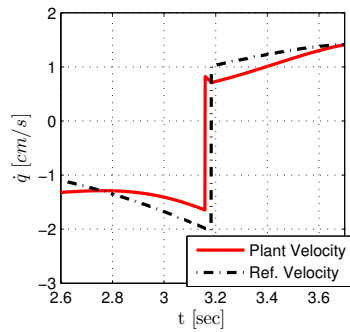

Figure 7.: Desynchronization of the reference trajectory with the plant trajectory for the undisturbed case.

5.4   *Impact Synchronization via Online Reference Model Reset*

In order to suppress the peaking phenomena, depicted in Fig. **??** and destroying the asymptotic stability of the disturbance-free closed loop system, the reference model is now reset online, as it is shown in the block-diagram of Fig. **??**. The idea behind such a reset is in using the same hybrid Van der Pol reference model of Section **??**, but instead of using its own unilateral constraint $q^r = 0$, the reset event is synchronized with the impact of the plant ($q = 0$). Thus, the restitution law (**??**)
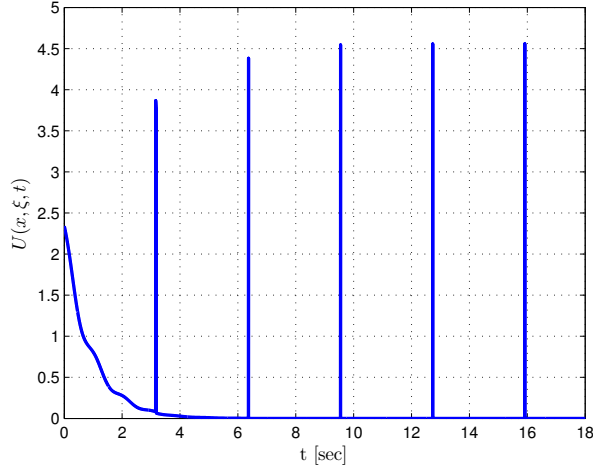
Figure 8.: Lyapunov function evolution in the disturbance-free case of the desynchronized tracking.

is modified to

$$q^r(t_i^+) = 0, \quad \dot{q}^r(t_i^+) = -e\dot{q}^r(t_i^-), \quad \text{iff } q(t_i) = 0. \tag{77}$$

The pre-feedback controller (??) and the same controller u, synthesized in Section ??, are now coupled to the Van der Pol reference model, thus modified. Hypotheses H1) - H3) are in force again, and it remains to show that H4) is additionally satisfied in the present case. Since the reference trajectory is reset when the plant hits the constraint, Scenario T3 is now in order, and due to (??), the error transition phase is governed by $x_2^+ = -ex_2^-$. It follows that $\|x^+\| \le \|x^-\|$ and H4) is thus established with V and W, specified in (32) and (34), respectively. This verifies the applicability of Theorem 2, by virtue of which, the properly specified dynamical controller (37) enforces the disturbance-free MSDB system to asymptotically track the reference trajectory while also attenuating external disturbances.

In order to demonstrate that the closed-loop system (??), (??), (??), (??), (37) generates an asymptotically stable limit cycle, the Poincaré analysis of Section ?? is revisited, using the Poincaré map

$$\tilde{\Gamma}(\zeta_k) = \zeta_{k+1} \tag{78}$$

associated with the Poincaré section $q = 0$, while considering the post-impact values $\zeta_k = [q_k, \dot{q}_k, \xi_k, q_k^r, \dot{q}_k^r]$ at the impact instants t_k, $k = 1, 2, \ldots$. The fixed point $\zeta^* = [0, 1.012, 0, 0, 0, 1.012]$ of the Poincaré map $\tilde{\Gamma}$ and the eigenvalues

$$eig(\nabla\tilde{\Gamma}) = [-0.1161, 0.1135, 0.0581 + 0.0204i, 0.0581 - 0.0204i, 0, 0] \tag{79}$$

of the gradient $\nabla\tilde{\Gamma}$ around the fixed point are numerically computed. The asymptotic stability of the a limit cycle, matching to the fixed point of the Poincaré map $\tilde{\Gamma}$, is then established by observing that eigenvalues (??) of the gradient $\nabla\tilde{\Gamma}$ are inside of the unit circle.

5.4.1   Numerical results

Figures ??-?? demonstrate the numerical results performed under the same circumstances as in Section ??, while the synthesized tracking controller is coupled to the Van der Pol reference model,
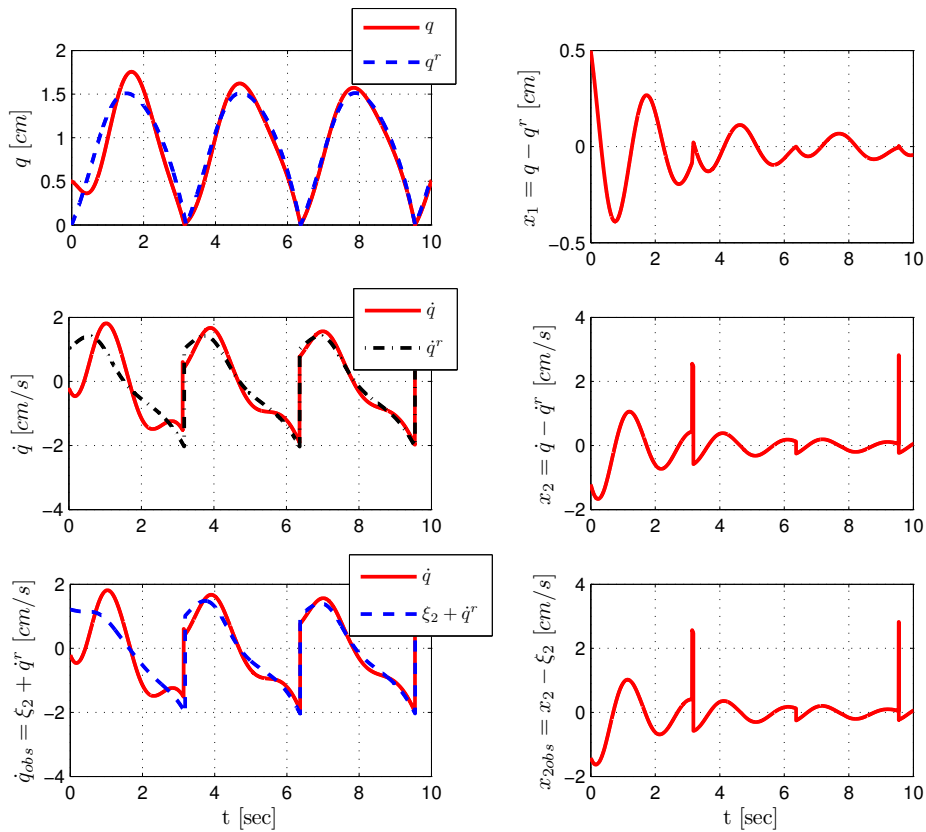
Figure 9.: Plots of the of the position and velocity tracking errors, and of the velocity estimation error for the disturbed case.

whose online reset adaptation is synchronized with the plant impacts. It can be seen from Fig. **??** that in the disturbance-free case, the position, velocity and estimation errors escape to zero regardless of nonzero initial conditions. The asymptotic stability of the closed-loop system can additionally be observed from Fig. **??** where the plotted Lyapunov function (17), specified with (32), (34), and (**??**), monotonically escapes to zero. The asymptotic stability of the limit cycle, theoretically predicted by the Poincaré analysis, is illustrated in Fig. **??**, where the plant trajectory (dashed line) converges to a periodic orbit (solid line).

The simulations, performed in the disturbed case, are reflected in Fig. **??** that depicts the plots of the position and velocity tracking errors as well as the plot of the velocity estimation error. It is seen that after the transitory, the errors remain small and bounded. As seen in Fig. **??**, this ensures that the plant trajectory evolves around the periodic orbit.

It is worth noticing that in both disturbed and undisturbed cases, the peaking effects of Fig. **??**, matching to the desynchronized impact instants of the plant and of the reference model, disappear from the velocity tracking and velocity estimation errors of Figs. **??** and **??** where the reference model resets are synchronized with the plant impact instants. Thus, the superiority of the synthesis with the online reference model reset adaptation is concluded.
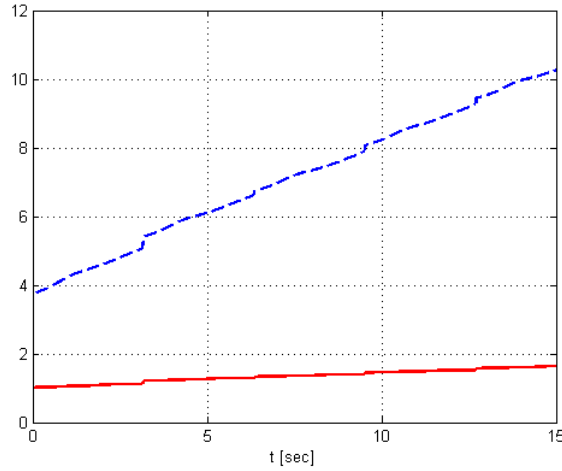
Figure 10.: $\mathcal{L}_2$-gain behavior without online reference model reset: $\|z\|_{L_2}^2 + \|z^d\|_{l_2}^2$ (solid line) vs. $\gamma^2[\|w\|_{L_2}^2 + \|w_i^d\|_{l_2}^2] + \Sigma_{k=0}^{N}\beta_k$ (dashed line) with $\gamma = 2$.
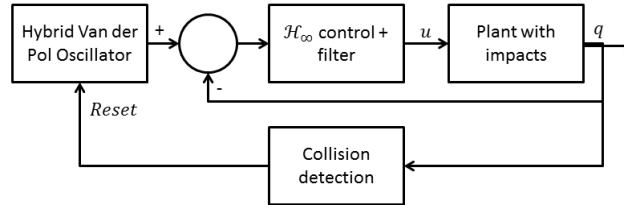

Figure 11.: Block-diagram of online Van der Pol reference model reset

.

6. A Case Study: Tracking of a Biped with Feet Using State Feedback Design

Theoretical results developed so far are now supported in the numerical study made for the robust trajectory tracking of a seven-link bipedal robot. The bipedal robot considered in this section is walking on a rigid and horizontal surface. It is modeled as a planar biped, which consists of a torso, hips, two legs with knees and feet. The walking gait takes place in the sagittal plane and is composed of single support phases and impacts which occur between two rigid bodies.

In the single support phase, considering a flat foot contact of the stance foot with the ground (i.e. there is no take off, no rotation, and no sliding during this phase), the dynamic model of the biped is a particular case of (39) where $\mathbf{q} = (q_1, q_2, q_3, q_4, q_5, q_6)^\top$ is the 6×1 vector of generalized coordinates, $\mathbf{D}$ is the symmetric, positive definite 6×6 inertia matrix, $\mathbf{D}_\tau$ is a 6×6 constant and non-singular matrix; $\boldsymbol{\tau} = \mathbf{\Gamma} = (\Gamma_1, \Gamma_2, \Gamma_3, \Gamma_4, \Gamma_5, \Gamma_6)^\top$ is the 6×1 vector of joint torques (see Fig.??); the term $\mathbf{H}(\mathbf{q}, \dot{\mathbf{q}})$ is the 6×1 vector of the centrifugal, Coriolis and gravity forces; and $\mathbf{w_1}$ is the 6×1 vector of external disturbances.

Now, assuming a flat foot contact of the swing foot landing on the ground, the double support phase is instantaneous and it can be modeled through passive impact equations.This impact is assumed to be absolutely inelastic and the feet are assumed not to slip.

For the sake of brevity, the description of the nonlinear model of the biped and the simulation method used to get the numerical results have been omitted. For more details reader can see the work by ?. In turn, the walking gait, which is composed of single support phases and impacts, is determined using the off-line optimization described in ?, thus generating a reference trajectory whose position $\mathbf{q^r}(t)$ and velocity $\dot{\mathbf{q}}^\mathbf{r}(t)$ satisfy the conditions of contact previously described.
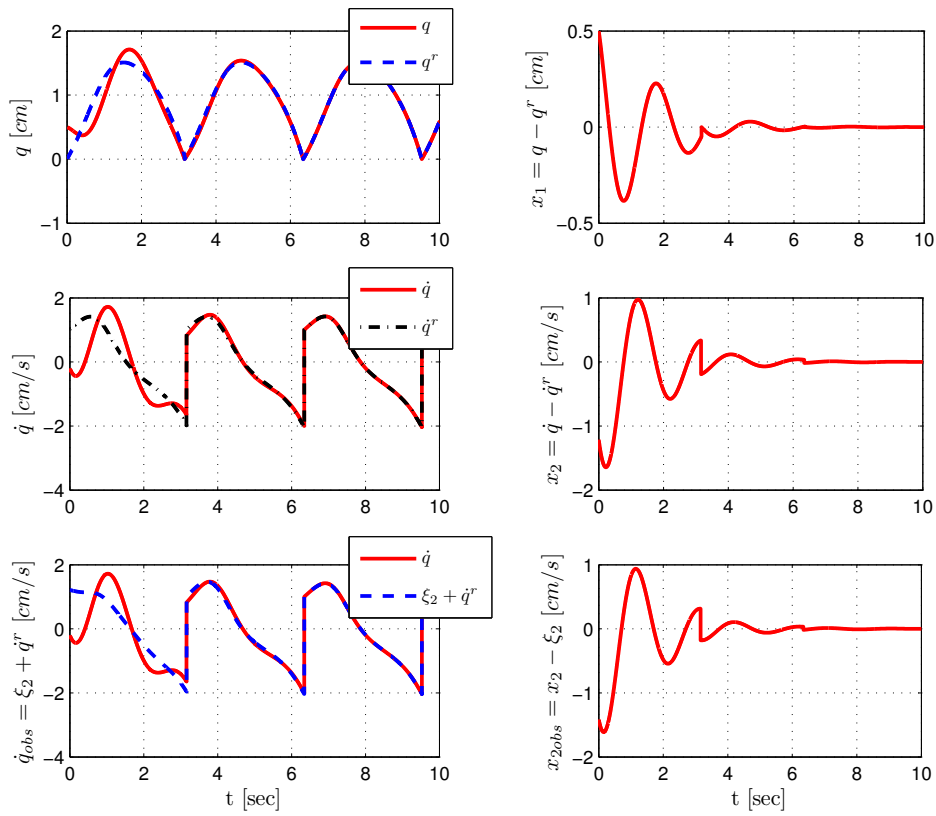
24

Figure 12.: Plots of the position and velocity tracking errors, and that of the velocity estimation error in the disturbance-free case when the online reset adaptation of the Van der Pol reference model is enforced.
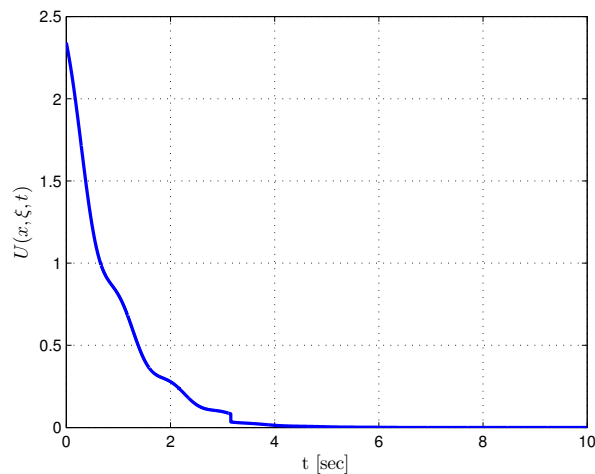
.

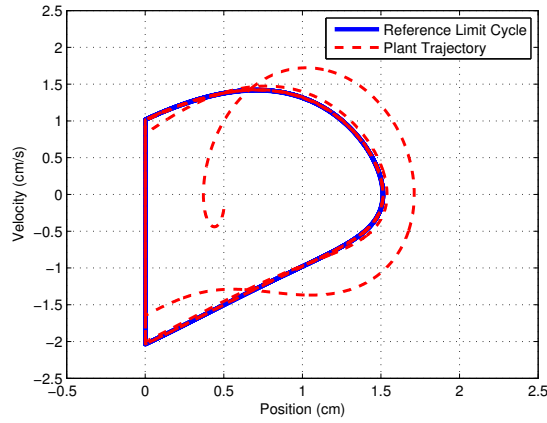Figure 13.: Lyapunov function evolution in the disturbance-free case of the synchronized tracking.

.

25

Figure 14.: Limit cycle of the synchronized impact Van der Pol Oscillator and a closed-loop plant trajectory, approaching it: the disturbance-free case

.

6.1 *State Feedback $\mathcal{H}_\infty$ Tracking Control Synthesis Using Reference Trajectory Adaptation*

The reference trajectory tracking synthesis of Sect. 4, being applied to the seven-link biped, is tested under the complete knowledge of the state vector. In order to respect Condition C1 of Theorem 3 for the error system (??) the to-be-controlled output (44) is specified with $\rho_p = 500$ and $\rho_v = 1$, and then, following the standard $\mathcal{H}_\infty$ design procedure (see, e.g., (?, Section 6.2.1)), the disturbance attenuation level and the perturbation parameter are set to $\gamma = 470$ and $\epsilon = 0.01$ to ensure an appropriate solvability of the perturbed differential Riccati equation (30), corresponding to (29), (??)-(??). Hypothesis H1) of Theorem 3 is then straightforwardly verified with γ, thus specified, and with $\boldsymbol{\omega}$, being an identity matrix. Finally, to comply with the last condition of Theorem 3 (inequality (14)) to be verified at the impact time instants, the reference trajectory is adapted on-line in such a manner that the state error dynamics possess no jumps. Thus, hypothesis H4) becomes redundant for the adapted trajectory because only trivial transitions with $\boldsymbol{\mu_0}(\mathbf{x},t) = 0$ are feasible in accordance with Scenario 3 of Section 4.1.

The idea of the above adaptation is presented in Fig.?? for the first joint q_1. Provided that the impact is detectable (e.g., by using a force or touch sensor) it happens that either the reference trajectory hits the constraint before the plant does, or the plant hits the constraint before the reference trajectory does. In the former scenario, the reference trajectory is continuously extrapolated until the plant collision occurs whereas in the latter scenario, the reference trajectory is restarted on-line once the plant collision is detected. Either way, both the plant trajectory and the adapted reference trajectory exhibit impacts at the same time instants. By adaptation, the nominal reference trajectory and the adapted one are equivalent before a collision. The position and velocity tracking errors are measured, and once the impact of the plant is detected, the adapted trajectory is updated on-line in such a manner that the new post-impact error, x_{21}^+ in Fig.??, coincides with the error measured before the impact ($x_{21}(t^l-)$ in Fig.??), thereby rendering the evolution of the error to exhibit no jump. Following the idea of ?, a new polynomial is defined for the adapted trajectory, that starts from this imposed condition, and will join the nominal reference trajectory at the middle of the step with the same velocity, and will continue to be the same until the end of the step. While the reference trajectory is recalculated after the impact, the perturbed differential Riccati equation (30) is also updated and its corresponding solution is recomputed on-line.
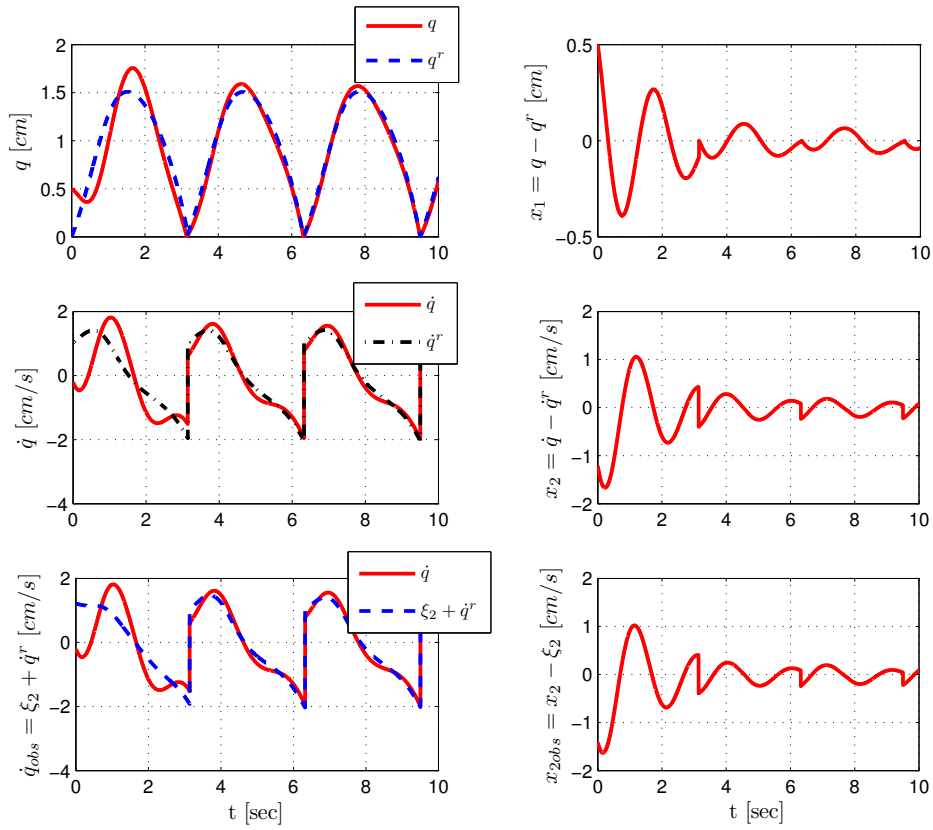
Figure 15.: Plots of the position and velocity tracking errors, and of the velocity estimation error in the disturbance-free case when the reference model is reset online.
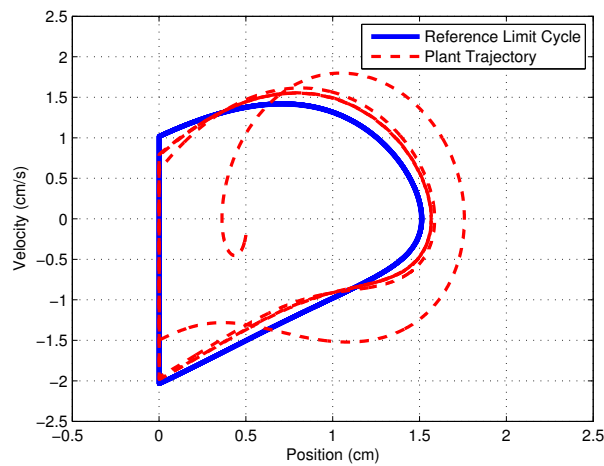

Figure 16.: Limit cycle of the synchronized impact Van der Pol Oscillator and a closed-loop plant trajectory, evolving around it in the presence of disturbances.
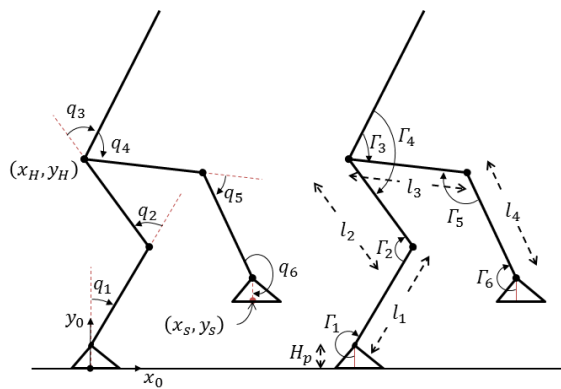
27
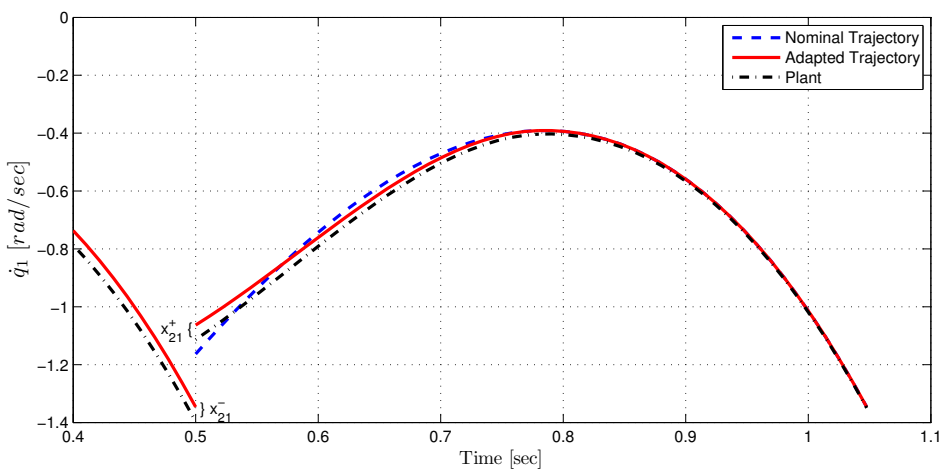
Figure 17.: Seven-link bipedal robot

Figure 18.: Reference velocity adaptation for the first joint, with an impact at $t^l = 0.5$. After the impact, the initial value of the adapted velocity is such that the pre-impact $(x_{21}(t^l-) = \dot{q}_1(t^l-) - \dot{q}_1^r(t^l-))$ and post-impact $(x_{21}(t^l+) = \dot{q}_1(t^l+) - \dot{q}_1^r(t^l+))$ tracking errors are the same, and at the middle of the step, the adapted reference velocity reaches the nominal one.

6.1.1 Numerical Results

In order to illustrate the performance issues of the developed stable bipedal gait synthesis numerical simulations were performed for a laboratory prototype whose parameters were drawn from **?**. The contact constraints presented in section 6.1 were verified on-line in order to confirm the validity of (39)-(43).

The undisturbed system was then simulated, using initial conditions different from zero ($\mathbf{q_0} = [0.1962, 0.2262, -0.0766, -0.1337, -0.1661, 0.0500]^\top$, $\dot{\mathbf{q}}_0 = [-1.0633, -0.6369, 0.3775, -0.3968, -1.4030, -1.4264]^\top$), so the plant is started away from the reference trajectory. Figure **??** shows three representative joints positions of the undisturbed system for twelve consecutive steps. It can be seen that these joints possess periodic trajectories. Using the reference trajectory adaptation method proposed, the velocity error is smooth and goes to zero, instead of presenting the peaking phenomena described in **?**. This is clearly observed in Fig.**??**a). Since there are no jumps in the velocity error, the Lyapunov function monotonically decreases to zero, as shown in Fig.**??**b). Figure **??** depicts the resulting heights of the feet. The periodicity of these heights is a good indicator of a stable motion for the walking gait. In Fig.**??**, legends "P1" and "P3" represent the "toe" of the right foot and left foot, respectively; similarly,

"P2" and "P4" represent the "heel" of the right foot and left foot.
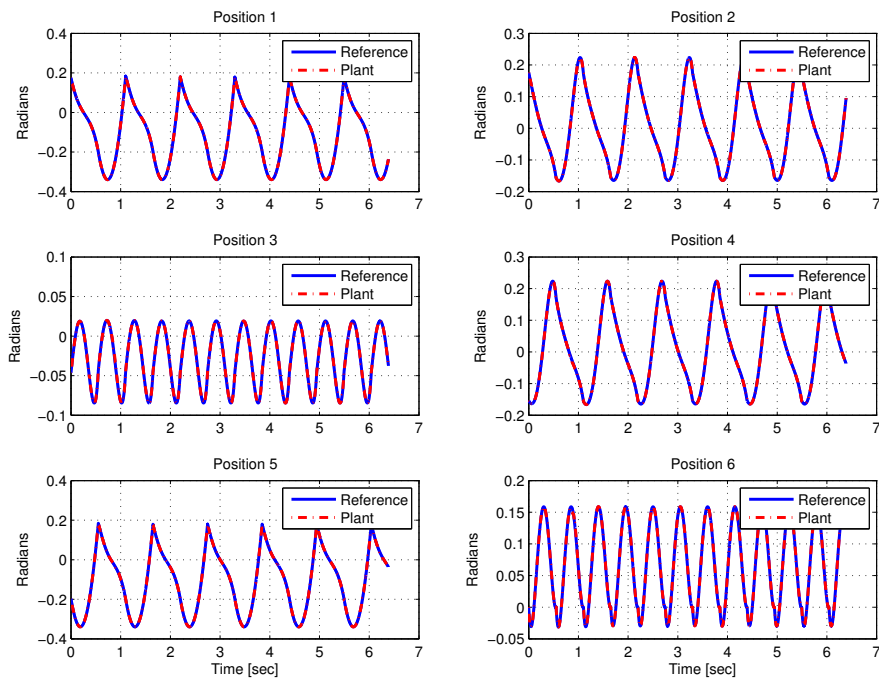

Figure 19.: Joints positions for the undisturbed system: the tracking error is zero for all joints

The robustness of the tracking controller (38) was tested by involving a resultant disturbance force $F_{xw} = 80$ N in the horizontal plane, applied to the hip of the robot. Such a force was used for the duration of 0.07 s to simulate a disturbance effect. This force, applied at 0.8 s in the first cycle of the biped, represented a disturbance in the continuous phase of the dynamics (39). The disturbances in the impact phase are introduced by modifying the velocities a 5% from their nominal values just after an impact occurs, to simulate the effect of uncertainties in the restitution law.
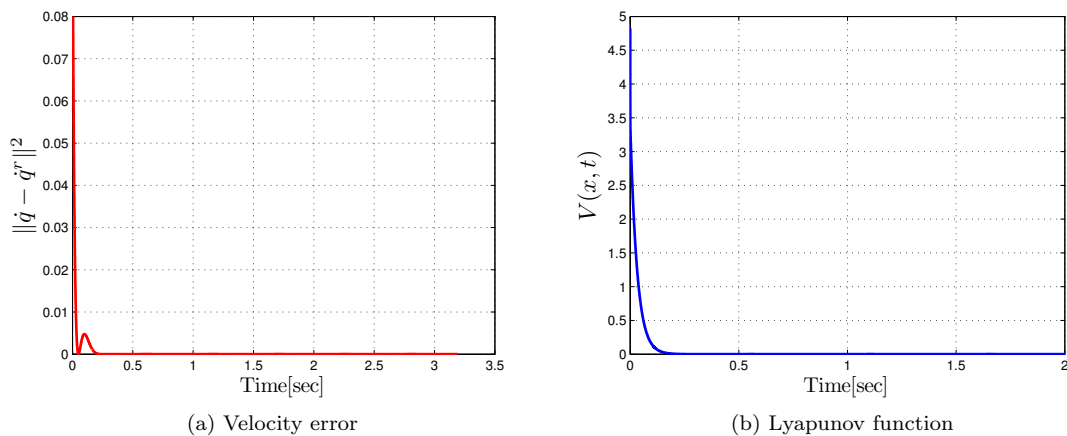

(a) Velocity error

(b) Lyapunov function

Figure 20.: Velocity error $\|\dot{\mathbf{q}} - \dot{\mathbf{q}}^{\mathbf{r}}\|^2$ and Lyapunov function (32) for the undisturbed system, initialized with nonzero conditions
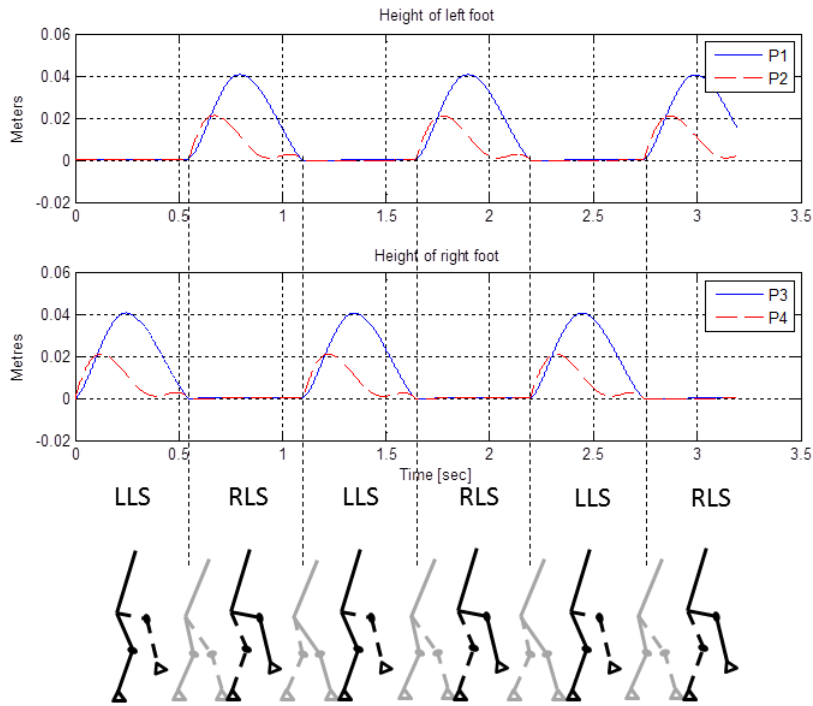
Figure 21.: Feet height in the walking gait, representing a stable motion with left leg support (LLS) phases followed by right leg support (RLS) phases, separated by impacts.
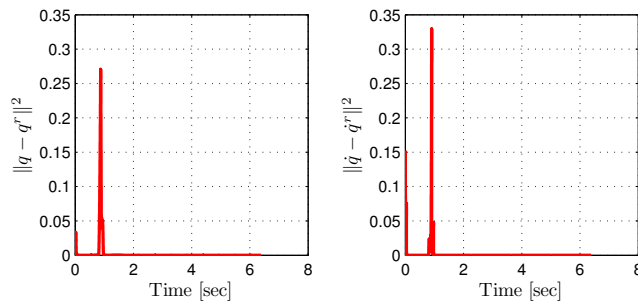

Figure 22.: Position and velocity errors $\|\mathbf{q} - \mathbf{q^r}\|^2$ and $\|\dot{\mathbf{q}} - \dot{\mathbf{q^r}}\|^2$ of the disturbed system. The effect of the disturbance is evident at 0.8 *sec*, and it is quickly attenuated by the controller.

The effect of the disturbance is observed in Figs.**??-??**. The disturbance attenuation is readily concluded from Fig.**??** where the effect of the disturbance is quickly attenuated by the controller. This effect is not evident in the feet heights plot, but the corresponding location of the Zero Moment Point (ZMP), depicted in Fig.**??**, directly reflects the disturbance effect which does not however influence on the stability of the walking gait because (see **?** for details) the ZMP location remains inside the support foot area between the toe and the heel. As predicted, the torques do not exhibit jumps due to the trajectory adaptation. In addition, one can observe from Fig.**??** that while attenuating the applied disturbance, the torques remain within the actuator limitations $(+/-150\ Nm)$. Once the discrete disturbance disappears the biped returns to its desired gait. Good robustness features are thus concluded from Figs.**??-??**.
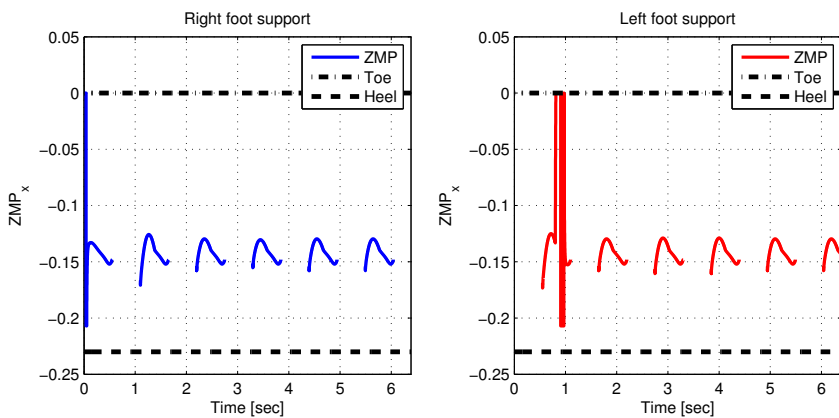
Figure 23.: Zero moment point (ZMP) location along the x-axis for each foot during its support phase. It is seen that the ZMP is always located between the toe and the heel of the supporting foot, so the walk is stable **?**.

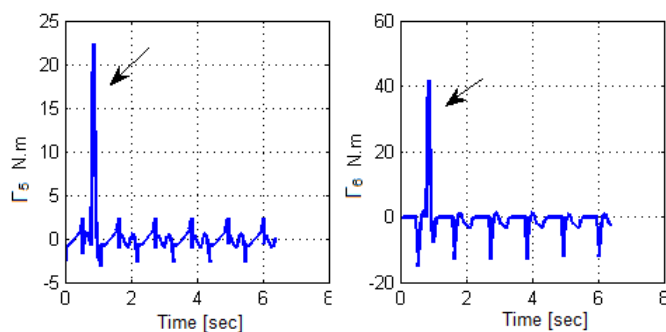Figure 24.: Torques appearing in joints 5 and 6, where the effects of the disturbance, pointed out by the arrows, are evident.

7.   Conclusion

In this paper, the $\mathcal{H}_\infty$-tracking/regulation problem is solved for mechanical systems under unilateral constraints via state and output feedback designs. Sufficient conditions for a local solution of the output feedback tracking problem to exist are obtained in terms of the appropriate solvability of an independent inequality on discrete disturbance factor that occurs in the restitution rule, and three coupled inequalities, involving two Hamilton-Jacobi-Isaacs inequalities. The former inequality ensures that the impulse dynamics (when the state trajectory hits the unilateral constraint) are ISS whereas the latter inequalities, arising in the continuous time state-feedback and, respectively, output-injection designs, should impose the desired iISS property on the continuous closed-loop dynamics between impacts. Once the state feedback is available, the number of the inequalities to be solved is reduced by one as the output injection is not required anymore.

The effectiveness of the resulting design procedure, which is based on solving disturbed differential Riccati equations, corresponding to the linearized system, is supported in the numerical study made for a benchmark (mass-spring-damper-barrier) system. The reference trajectory to follow is generated by an impact Van der Pol oscillator, possessing an asymptotically stable limit cycle. The desired disturbance attenuation is satisfactorily achieved under external disturbances during the free-motion phase and in the presence of uncertainties in the transition phase. An online reference model reset adaptation is additionally applied in order to synchronize the impacts of the plant with those of the reference model, thereby enhancing the performance of the closed-loop system.

The practical value of the resulting local synthesis is additionally validated in the numerical study of the stable gait synthesis of a seven-link biped emulator. It is shown, that the desired disturbance attenuation is satisfactorily achieved under external disturbances during the free-motion phase and in the presence of uncertainty in the transition phase.